Forest Ecology and Management 615 (2026) 123843

Contents lists available at ScienceDirect

Forest Ecology and Management

journal homepage: www.elsevier.com/locate/foreco

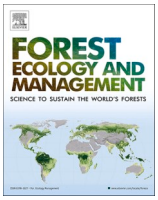

Decadal climate-driven decoupling between gross primary productivity and tree growth in Mediterranean forests

Daniela Dalmonech [a,b,*], Elia Vangi [a,c], Dánnell Quesada Chacón [d], Alessio Collalti [a,b]

[a] Forest Modelling Laboratory, Institute for Agriculture and Forestry Systems in the Mediterranean, National Research Council of Italy (CNR-ISAFOM), Via Madonna Alta 128, Perugia 06128, Italy
[b] National Biodiversity Future Centre (NBFC), Piazza Marina 61, Palermo 90133, Italy
[c] geoLAB - Laboratory of Forest Geomatics, Dept. of Agriculture, Food, Environment and Forestry, Università degli Studi di Firenze, Via San Bonaventura 13, Firenze 50145, Italy
[d] Potsdam Institute for Climate Impact Research (PIK), Potsdam 14412, Germany

ARTICLE INFO

Keywords:
Mediterranean forests
Tree growth
Photosynthesis
Decoupling
Modelling

ABSTRACT

Mediterranean forests are becoming increasingly vulnerable under climate change, as the growing frequency and intensity of droughts and heatwaves amplify physiological stress, reduce productivity, and heighten the risk of large-scale disturbances. However, vegetation activity trends derived from remote sensing may mask divergent responses between photosynthetic activity and growth, which represent a critical early warning signal of forest vulnerability. Therefore, the long-term relationship between photosynthesis and tree growth remains poorly understood at regional scales, especially in Mediterranean areas. To address this challenge, we applied a mechanistic, process-based forest ecosystem model across approximately 2400 km^2 of typical Mediterranean forests in southern Italy, encompassing a heterogeneous landscape characterized by diverse stand structures and species dominance. This framework enabled to explicitly trace carbon fluxes from gross primary productivity (GPP) through allocation processes to average tree growth. Using a factorial approach, we identify, over large spatial scales, an emergent pattern of divergence between summer GPP and radial tree growth, amplified in space and time by climate variability over the last two decades and further shaped by forest legacy effects. Our findings also reveal that canopy-level greening can mask structural vulnerability and pre-visual decline across Mediterranean forests. Data show that an apparent long-term trend in photosynthesis decline during summer does not necessarily translate to tree growth decline. Improving our ability to determine if, where and when a key change in forest behaviour will occur, remains essential for designing effective restoration measure and anticipating tipping points in forest resilience under accelerating climate change.

1. Introduction

Over recent decades, global forests have exhibited a progressive decline in their capacity to function as effective carbon sinks (Forzieri et al., 2022; Pan et al., 2024). This weakening of the forest carbon sink arises from the combined effects of direct anthropogenic disturbances, such as forest harvesting and biomass removal, and an increasing frequency and intensity of change-driven natural disturbances, including droughts, heatwaves, storms, and pest outbreaks (Knutzen et al., 2025; Migliavacca et al., 2025; Grünig et al., 2026). Since 2000, large areas of European forests have experienced more frequent and severe extreme events, particularly heat waves, and droughts (Lhotka and Kyselý, 2022; Ossó et al., 2022; Xu et al., 2020). Understanding how recurrent extreme events alter carbon fluxes, and the extent to which forest responses mediate these changes, is crucial for monitoring and assessing forest ecosystem functioning. Such knowledge is essential for designing and implementing effective restoration strategies in vulnerable forests, ensuring the recovery and conservation of forest carbon sinks, and thereby supporting the European Union's climate change adaptation and biodiversity objectives (Chapman et al., 2025; Svensson et al., 2025).

Long-term trends in warming and decreasing precipitation levels, coupled with increasing atmospheric dryness, have threatened forest health and growth across Europe and other regions (Samaniego et al.,

* Corresponding author at: Forest Modelling Laboratory, Institute for Agriculture and Forestry Systems in the Mediterranean, National Research Council of Italy (CNR-ISAFOM), Via Madonna Alta 128, Perugia 06128, Italy.
E-mail address: daniela.dalmonech@cnr.it (D. Dalmonech).

https://doi.org/10.1016/j.foreco.2026.123843
Received 25 February 2026; Received in revised form 25 April 2026; Accepted 27 April 2026
Available online 5 May 2026

2018; Sanginés de Cárcer et al., 2018; Yuan et al., 2019; Martinez del Castillo et al., 2022). In southern Europe, the anthropogenic climate signal is becoming increasingly evident (IPCC, 2023), with extremes intensifying in both frequency and magnitude. The Mediterranean basin, recognized as a climate change hotspot, is particularly vulnerable: drought strongly affects both socioeconomic systems (Noce et al., 2016; Tramblay et al., 2020) and forest functioning, especially where tree species live at their southern distribution or rear-edge limits (Noce et al., 2017). Although Mediterranean tree species are often considered drought-adapted (Joffre et al., 2007), projected higher warming rates with increased frequency and intensity of extreme weather events under future climate scenarios are expected to worsen drought-induced dieback, tree defoliation, and impair tree growth (Gazol and Camarero, 2022; Molina et al., 2020; Petritan et al., 2021; Ripullone et al., 2020). Relationships have been demonstrated between lower growth rates, i.e., decline in basal area increment (BAI), and tree mortality risk (Cailleret et al., 2017; DeSoto et al., 2020; Vayreda et al., 2012), potentially predisposing forests to severe drought impacts (Neycken et al., 2024).

Tree growth responses to environmental variability arise from the complex interplay and co-variation of multiple abiotic and endogenous biotic factors. Species-specific functional traits, eco-physiological characteristics, and carbon allocation strategies (Decarsin et al., 2024), together with edaphic conditions (Gessler et al., 2018; Sterck et al., 2024) regulate tree growth dynamics. In addition, forest structure and demographic processes (Astigarraga et al., 2025; Wang et al., 2024) shape trees' capacity to withstand stress and to recover following stress-induced growth declines. Estimates of temporal trends in tree ring data have already proven effective for interpreting growth rate changes in relation to climate change (Piovesan et al., 2008; Schurman et al., 2019; Shestakova et al., 2016). However, dendrometric monitoring is expensive, time-consuming, and spatially sparse, thereby limiting the capacity to assess drought impacts consistently across Mediterranean regions (Tramblay et al., 2020).

Remote sensing data can partially address vegetation monitoring challenges at large scales, over long time periods, and at high resolution (Bathiany et al., 2025). Long satellite records can provide decadal canopy-level assessments, revealing for instance widespread greening at large scales, modulated by land use and land cover change, increasing atmospheric CO_2 concentration and temperature but down-regulated by vapor pressure deficit (Zhu et al., 2016; Yuan et al., 2019). However, canopy-level greening can mask localized mortality events and disturbances (e.g. Yan et al., 2024) and tree decline may precede any detectable canopy-level signal (Neycken et al., 2022; van der Maaten et al., 2024). Vegetation may respond rapidly and negatively to extreme conditions such as summer drought, typically captured at very fine scales in the form of local canopy-level damage, while vegetation state might remain largely unaffected as plants can sustain near-complete recovery at the canopy level (e.g., Italiano et al., 2024; Pollastrini et al., 2019). Hence, climate change and extremes can impact forest ecosystem compartments, e.g. canopy, living biomass, differently and with varying degrees of delay (Kannenberg et al., 2020), thereby posing challenges for monitoring and forecasting near-future forest states and potential tipping point in forest resilience. To overcome the limitations of dendroecological and remote sensing approaches, we use a state-of-the-science biogeochemical, biophysical, process-based forest model to simulate long-term forest dynamics in a Mediterranean region at both canopy and tree levels, including wood formation (Friend et al., 2019). The use of a mechanistic approach to investigate co-occurring trends in gross primary productivity (GPP) and tree growth has proven promising (e.g., Gea-Izquierdo et al., 2017; Puchi et al., 2026). In this context, modelling approaches provide a valuable and complementary line of analysis, helping to overcome the spatial and temporal fragmentation typically associated with ground-based observations (e.g., Klesse et al., 2018). Simulated forest carbon dynamics and overall stand-level functioning emerge from the internal feedback and interactions among individual biotic and abiotic processes that are mechanistically represented within the forest models (Boukhris et al., 2025) In addition, stand-level forest models have been developed for impact studies at higher resolution than their regionally- or globally-resolved counterparts (e.g., ISIMIP; Reyer, 2015), to explicitly consider forest structure and management in order to make predictions (Collalti et al., 2018; Dalmonech et al., 2022; Testolin et al., 2023; Saponaro et al., 2025). In this study, we apply the process-based forest ecosystem model 3D-CMCC-FEM at the regional scale across representative Mediterranean forest ecosystems in southern Italy (Basilicata region). Vegetation activity is quantified through GPP and stand-average BAI, capturing both carbon assimilation and biomass accumulation processes. The simulations span nearly two decades (2005–2023) and are designed to disentangle and assess the relative contributions of carbon assimilation and woody biomass allocation to tree growth. These processes are examined in the context of their modulation by interacting abiotic drivers, such as climate, and biotic drivers, including stand structure and species dominance. Specifically, we address two questions: (1) through which mechanistic pathways does climate forcing influence carbon assimilation, allocation, and growth, and how do these interactions determine long-term tree dynamics in Mediterranean forests?; (2) How do forest structure and species shape the climate-induced response of carbon sink and source? Limitations and challenges are also discussed.

2. Material and methods

2.1. Climatological data and atmospheric CO_2

The climate data used in this study were obtained from the ERA5-Land dataset (Muñoz-Sabater et al., 2021), a high-resolution (0.1° horizontal resolution) land-surface reanalysis produced by the European Centre for Medium-Range Weather Forecasts (ECMWF). ERA5-Land provides hourly data on various land-surface variables, including temperature, precipitation, and surface pressure, among others. Variables not directly available in ERA5-Land were derived from existing data at hourly temporal resolution. Specific humidity (huss) and relative humidity (hurs) were derived using near surface dewpoint temperature, surface pressure (ps), and near-surface air temperature (tas), based on the equations outlined by Buck (1981) and further detailed in Buck Research Instruments LLC (2010). Wind speed (sfcWind) was derived from eastward near-surface wind (uas) and northward near-surface wind (vas) according to sfcWind = sqrt(uas * uas + vas * vas). Sea level pressure over land was computed from the orography (orog), ps, and tas according to psl = ps * exp((g * orog) / (r * tas)), where g is gravity, and *r* is the specific gas constant of dry air. The hourly data were then aggregated to daily values, including minimum (tasmin), maximum (tasmax), mean (tas, ps, psl, hurs, huss, sfcWind), and daily cumulative totals for precipitation (pr), snowfall (prsn), surface downwelling longwave radiation (rlds) and surface downwelling shortwave radiation (rsds), similarly to Lange et al. (2021).

In this study we used tasmax, tasmin, pr, hurs, and rsds for the 1980–2023 period and data were resampled over the simulation grid at 1 km^2 by means of a bilinear interpolation.

Global annual atmospheric CO_2 concentrations were compiled from the NASA-observatory dataset (https://scripps.ucsd.edu/) for the period 1980–2023.

2.2. Study area

The study region, Basilicata, is located in southern Italy and is characterized by a typical Mediterranean climate, with hot summers and mild winters (Fig. 1a). The climate is predominantly humid in the Apennine mountains and dry over the hills and flat areas. Elevation gradient ranges from sea level to 2200 m above sea level, and annual precipitation spans from 500 to 2000 yr^{-1}.

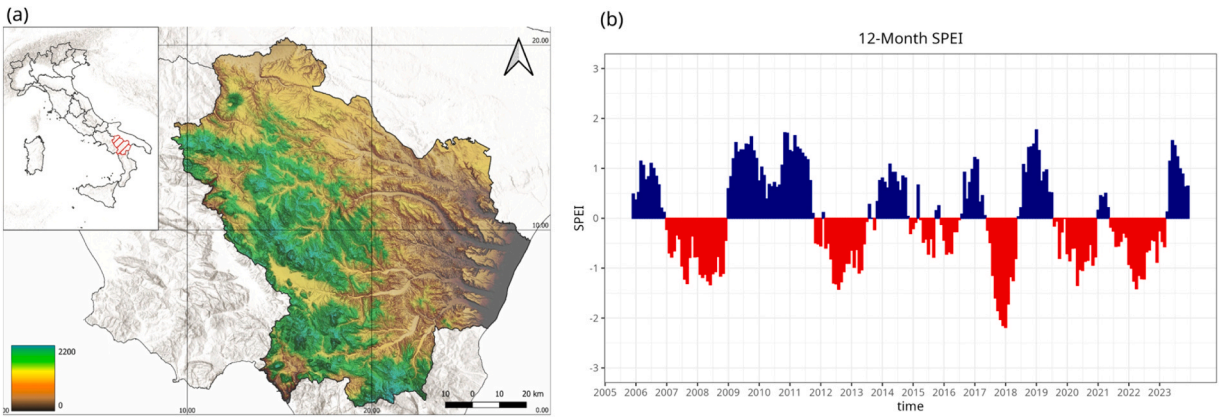

Fig. 1. a) Location of the study region in southern Italy; b) Standardized Precipitation Evapotranspiration Index (SPEI) computed at a temporal scale of 12 months from ERA5-Land meteorological data, representing the median value computed across the region. Blue and red indicate wetter and drier conditions than the long-term average, respectively. A SPEI value below −1 is used as the threshold of onset of mild to severe drought.

Forest cover accounts for 29% of the region and represents a broad range of geographical and geological variability, forest species and structure, capturing thus the heterogeneity typical of the forests in the Mediterranean basin (Geri et al., 2010; Vangi et al., 2025). Forests are dominated mainly by deciduous *Quercus ssp.* (63%), principally *Quercus cerris* L., primarily found in the hilly areas within the elevation belt 500–1000 m, *Fagus sylvatica* L.(~9%), covers mostly areas above 900 m elevation. Less abundant species include *Quercus ilex* L., (3.4%), *Castanea sativa* Mill., *Pinus halepensis* Mill. and *Pinus nigra* J.F. Arnold (2.5% and 0.9% respectively) as shown in Figure. S1. The primary forest structure is high forest or old coppice transitioning to high forest, ~58% of the forested area, while ~27% is managed as coppice (Costantini et al., 2006). The present-day climate in the Basilicata region embeds the fingerprints of the main extremes occurred in the last two decades, which also affected other European forests over large areas, such as the heatwaves and drought in years 2007, 2017, 2020 and 2022 (e.g. Lhotka and Kyselý, 2022; Rita et al., 2020) These conditions are described by the multi-scalar drought index SPEI (Standardized Precipitation Evapotranspiration Index; Vicente-Serrano et al., 2010), whose time series is reported in Fig. 1b.

2.3. The 3D-CMCC-FEM

2.3.1. Forest model description

GPP and BAI were simulated using the process-based forest model 3D-CMCC-FEM (*Three-Dimensional Coupled Model Carbon Cycle – Forest Ecosystem Module*, v.5.6; Collalti et al., 2024; Collalti et al., 2016; Dalmonech et al., 2022). The model prognostically represents the carbon and water cycles in forest ecosystems at stand and species level, explicitly simulating key biochemical and biophysical processes, such as photosynthesis, evapotranspiration, autotrophic rerpiration and, among the different pools, carbon allocation in woody biomass (e.g., Puchi et al., 2026; Saponaro et al., 2025). The model simulates the forest population dynamics with a cohort-based approach, and the eco-physiological dynamics are represented as responses to environmental drivers and external disturbances such as forest management. A carbon reserve pool, one of the seven tree-level carbon pools, acts as a buffer during periods of negative carbon balance, when plant respiration (both growth and maintenance respiration) exceeds GPP. This pool also plays a quasi-active role in regulating carbon allocation dynamics, influencing the partitioning of newly assimilated carbon among the fiferent carbon pools. The 3D-CMCC-FEM explicitly accounts for drought impacts, both edaphic and atmospheric, on tree physiology. Direct short-term effects are simulated through the modulation of stomatal conductance using the Jarvis model (Jarvis, 1976), through adjustments in carbon allocation pathways and defoliation. Long term effects arise from temperature-driven increases in metabolic respiration, which reduce plant reserve availability, potentially leading to carbon starvation and, ultimately, tree mortality (McDowell et al., 2008), one of the different ways in the model to simulate mortality. More details on the model are found in section S1 of Supplementary material and in Collalti et al. (2024). The 3D-CMCC-FEM has proven to be a valuable tool for forest ecosystem monitoring (Dalmonech et al., 2024; Vangi et al., 2025), for advancing process-level understanding of forest functioning (Collalti et al., 2020; Puchi et al., 2026; Saponaro et al., 2025), and for predictive applications under changing climatic conditions (Collalti et al., 2018; Dalmonech et al., 2022; Testolin et al., 2023; Vangi et al., 2024). The model has been extensively tested and evaluated over a broad range of climates and species, at local (Testolin et al., 2023), regional (Dalmonech et al., 2024) and the national scale (Vangi et al., 2025).

At the national scale across Italian forests, the model was evaluated against more than 5000 National Forest Inventory plots (Vangi et al., 2025), successfully reproducing average diameter at breast height and aboveground carbon stocks in the study region. In a European model intercomparison (Mahnken et al., 2022), it ranked among the best-performing models in simulating GPP sensitivity to daily meteorology. Additional support from Puchi et al. (2026) further demonstrates the model's ability to capture interannual variability in ecosystem fluxes and stem carbon allocation.

2.3.2. Forest model initialization and simulations

The 3D-CMCC-FEM was applied over the regional grid at a spatial resolution of 1 km^2. Initial forest structure was derived for year 2005 from the second Italian National Forest Inventory (NFI) and further refined using high-resolution regional maps of forest and land-use cover, as already described in Dalmonech et al. (2024). This approach allowed the model to capture spatial heterogeneity in species occurrence, age distribution, and biomass pools, ensuring that stand-level structural variability and ecological characteristics were adequately represented across the simulated landscape. For each grid cell, a representative forest stand was simulated as a single cohort defined by the most dominant species, hereinafter indicated as 'forest class', along with its average diameter at breast height (DBH), average stand density (trees ha^{-1}) and age. The key species considered in this study were: European beech (*Fagus sylvatica*), Black pine (*Pinus nigra*), Sweet chestnut (*Castanea sativa*), Turkey oak (*Quercus cerris*), Aleppo pine (*Pinus halepensis*), and Holm oak (*Quercus ilex*).

Soil characteristics, namely soil texture and soil depth, were extracted from a detailed regional pedological map and the Italian soil map CREA-db (Costantini and Dazzi, 2013). Following the model simulation protocol as in Dalmonech et al. (2024), a prescribed constant

percentage of the annual thinning rate was applied to forested areas outside protected areas, and areas affected by fire during the simulation period were excluded from the analyses. The total modelled area encompassed approximately 2400 km^2. The 3D-CMCC-FEM was forced with daily meteorological data, including maximum and minimum temperatures, precipitation, relative humidity and shortwave downwelling radiation and together with global atmospheric CO_2 concentration (2.1). Simulations were performed from 2005, the first year of forest structural data availability, until 2023 representing the "present-day" scenario. To compare and isolate the climate variability effect on forest dynamics under present day from the intrinsic biological stand development, we created an ensemble of three baseline forcing scenarios by randomly sampling years from the 1980–2004 ERA5-land meteorological record, following the approach of Collalti et al. (2018); in the baseline scenarios, atmospheric CO_2 concentration was held constant as its 2005 value.

BAI was used as a proxy for average tree-level growth, partially reducing the age- and size-related effects (Biondi and Qeadan, 2008). Specifically, BAI was computed from the simulated average DBH assuming a circular stem cross-section, as follows:

$$\mathrm{BAI} = \pi\left(r_i^2 - r_{i-1}^2\right) \text{ with } i = \text{year of simulation}$$

2.3.3. Forest model parameterization

Unlike some other vegetation models that require a spin-up phase until vegetation reaches equilibrium with climate conditions, the 3D-CMCC-FEM is initialized directly from observational-based estimates of forest structure. Prescribing initial conditions alone constitutes a major constraint on the simulated trajectories of forest ecosystem models. Species-specific eco-physiological model parameterization was taken from Vangi et al. (2025). Allometric equations (e.g. linking tree DBH and canopy height) were calibrated on site-level data from the region, following Dalmonech et al.(2024). An in-depth 3D_CMCC_FEM sensitivity analysis to parameters was described in Collalti et al. (2019), identifying key parameters, particularly those relating DBH to sapwood area and stem biomass. In this study, these parameters were calibrated by adjusting their values by up to ±10% from their standard values (Table S1). The model's ability to simulate vegetation trends was then evaluated.

2.4. Remote sensing-based data

Modelled vegetation activity in terms of gross primary productivity was compared against remote sensing (RS) observations. Due to uncertainties across different data (e.g. Sun et al., 2019), four different records were used. Selected vegetation indices were computed from Landsat images bands at 30-meter resolution and include: (i) the Enhanced Vegetation Index, EVI, (ii) the Normalized Difference Vegetation Index, NDVI and (iii) the Tasselled Cap Greenness, TCG (Crist and Cicone, 1984; Xue and Su, 2017; Jiang et al., 2008).

These vegetation indexes are widely recognised standards in remote sensing analyses, valued for their ability to provide consistent, quantitative information on vegetation status and dynamics (Xue and Su, 2017).

In particular, the NDVI delineates vegetation and vegetative stress by showing dense vegetation with high positive values, bare soil with low positive values, and water with negative values. The EVI is known for not saturating as rapidly as NDVI in dense vegetation and has been shown to be highly correlated with photosynthesis, plant transpiration, and vegetation biomass (Sims et al., 2006; Jiang et al., 2008). The TCG reflects the combined effects of intense absorption in the visible wavelengths caused by plant pigments and high reflectance in the near-infrared due to internal leaf structure and the associated scattering of near infrared radiation, NRI. This spectral pattern is typical of healthy green vegetation. TCG has been shown to correlate moderately to strongly with percent canopy closure, leaf area index, and fresh biomass.

Monthly image composites for the study area were generated by selecting the optimal pixel observations f from all available Landsat-5 TM, Landsat-7 ETM+ , and Landsat-8 OLI imagery using the Best Available Pixel (BAP) method (White et al., 2014). This method allows filling the final image mosaic with the best pixel according to four different scoring criteria: (i) acquisition day of the year (DOY), (ii) atmospheric opacity, (iii) distance to clouds and cloud shadows, and (iv) sensor type. Scores are summed and the pixel with the highest total score (i.e., the BAP) is selected for the final image composite. Images acquired within ±15 days of the target DOY with less than 50% cloud cover are considered viable candidates for compositing. The target DOY, was set to the 15th day of each month.

Data were made freely accessible via the Google Earth Engine from the United States Geological Survey (USGS; https://earthengine.google.com). Further details on the BAP image compositing approach are provided in Griffiths et al. (2013), and information on tuning parameters can be found in White et al. (2014).

We additionally selected the GOSIF-GPP dataset (Li and Xiao, 2019a), which provides global estimates of monthly GPP fluxes at 5 km resolution from solar-induced fluorescence (SIF) data retrieved by the Orbiting Carbon Observatory (OCO-2) satellite (Li and Xiao, 2019b). SIF is currently considered the most reliable large-scale proxy of plants' photosynthetic activity (Sun et al., 2018). All RS-based data were masked to the forest extent and resampled to the 1 km^2 simulation grid.

Modelled and RS-based agreement of spatial trends of vegetation activity was quantified using the integrated metric SPAtial EFficienty (SPAEF) metric (Koch et al., 2018) which include spatial correlation *(r)*, the coefficient of variation *beta* and the degree of histogram overlap, *gamma*, combined as SPAEF= $1 - \sqrt[2]{(\mathrm{r}-1)^2 + (\mathrm{beta}-1)^2 + (\mathrm{gamma}-1)^2}$. SPAEF ranges between $-\infty$ and 1, where 1 indicates perfect model-data agreement, and negative values indicate poor performances.

2.5. Decadal GPP-BAI analyses

Long-term trends (2005–2023) were computed for RS-based data, and the occurrence of positive and negative trends, was compared. The Theil–Sen estimator was applied to estimate the slope magnitude, and the statistical significance of the slope was assessed using the Mann-Kendall test, accounting for autocorrelation in the time series (Yue et al., 2002). Vegetation activity trends in both RS and modelled GPP were normalized to the average over the simulation period (2005–2023) and reported as percentages. Trends were computed from aggregated summer values, (June, July, and August), which provide the most robust signal across RS-based data and model output, as it captures the peak of the growing season and thus has a high signal-to-noise ratio (Leisenheimer et al., 2024). Additionally, confounding signals from understory vegetation (e.g., grass, evergreen shrubs) are reduced. The same trend analyses were performed based on the modelled GPP and BAI data under the present-day scenario and the baseline runs (see 2.3.2). In the latter case, BAI and GPP trends were averaged across the three runs to provide a single baseline scenario. Thereinafter in the text we simply refer to "baseline scenario".

To determine where and to what extent present-day climate variability, has affected long term trends of GPP and BAI over the last two decades, results under the present-day and baseline scenario" were compared.

We quantified the coupling strength between BAI and GPP by computing elasticity (De Kroon et al., 2000; Chiew, 2006), a non-dimensional metric that, in this study, describes the proportional change in BAI resulting from a proportional change in GPP. The elasticity was linearized and expressed as:

$$\text{Elasticity} \cong \frac{\Delta BAI}{BAI} \Big/ \frac{\Delta GPP}{GPP} \cong \frac{TREND_{BAI}}{BAI_{bs}} \Big/ \frac{TREND_{GPP}}{GPP_{bs}}$$

To reflect the change in decadal trend under the present-day climate variability, the BAI and GPP slope are normalized by the respective baseline means. Elasticity equal to 1 indicates a perfectly proportional response of BAI to GPP; values greater than 1 indicate that BAI responds more strongly than GPP under the same environmental conditions. To account for the cases where BAI and GPP trend slopes may have opposite sign, the final metric is computed as the absolute value of (Elasticity-1).

The metric is computed under both the baseline and under the present-day scenario. The difference between the two indicates how the coupling between BAI and GPP shifts in response to current climate conditions. Positive differences indicate decoupling, i.e. BAI responds proportionally less than GPP, while negative differences indicate strength of the coupling. Decoupling is considered weak when BAI and GPP trends share the same sign, and strong when their signs diverge (e.g. negative BAI trend paired with a positive GPP trend). The elasticity analyses are complemented by the identification of spatial "hotspots" of decoupling and divergent patterns of BAI and GPP trends. Results are aggregated on a regional map into four classes labeled as GPP^{pos}-BAI^{pos}, GPP^{pos}-BAI^{neg}, GPP^{neg}-BAI^{pos}, and GPP^{neg}-BAI^{neg} where superscripts indicate the sign of the trend.

Finally, we created a meta-model of the spatially simulated BAI trends at regional scales using a Random Forests model. This statistical model employs a machine learning technique, based on regression trees, that uses an ensemble of multiple individual random trees (Breiman, 2001). This algorithm was chosen for its robustness to collinearity among predictors and its ability to detect linear, nonlinear, and interacting effects among predictors. The algorithm was applied to the simulated BAI trend, training the statistical model with a list of selected spatial predictors. The selection of variables followed a parsimonious yet ecologically meaningful approach. Key climate predictors included the 2005–2023 spring and summer averages of maximum temperature, precipitation, and vapor pressure deficit, along with GPP and the 12-month SPEI as an aggregated drought measure (Vicente-Serrano et al., 2010). Abiotic predictors comprised soil depth, elevation, and soil clay percentage. Initial stand density, average DBH, and age class were also included as structural forest descriptors.

The final Random Forest model selection and cross-validation were carried out using the percentage of explained data variance metric (R^2). Predictor's importance and significance were assessed by the increase in mean squared error (incMSE) following variable permutation (Strobl et al., 2008). Partial dependence plots (PDPs) were used to visualize the marginal effect of the three most important predictors on BAI trends, averaging over the joint distribution of all remaining predictors (Friedman, 2001). Spatial autocorrelation effects were examined using Moran's I on the Random Forest model residuals.

Post-processing and statistical analyses were performed in R programming language (R Core Team, 2021) using the packages *RandomForest*, *rfPermute* and *pdp* (Liaw and Wiener, 2002)

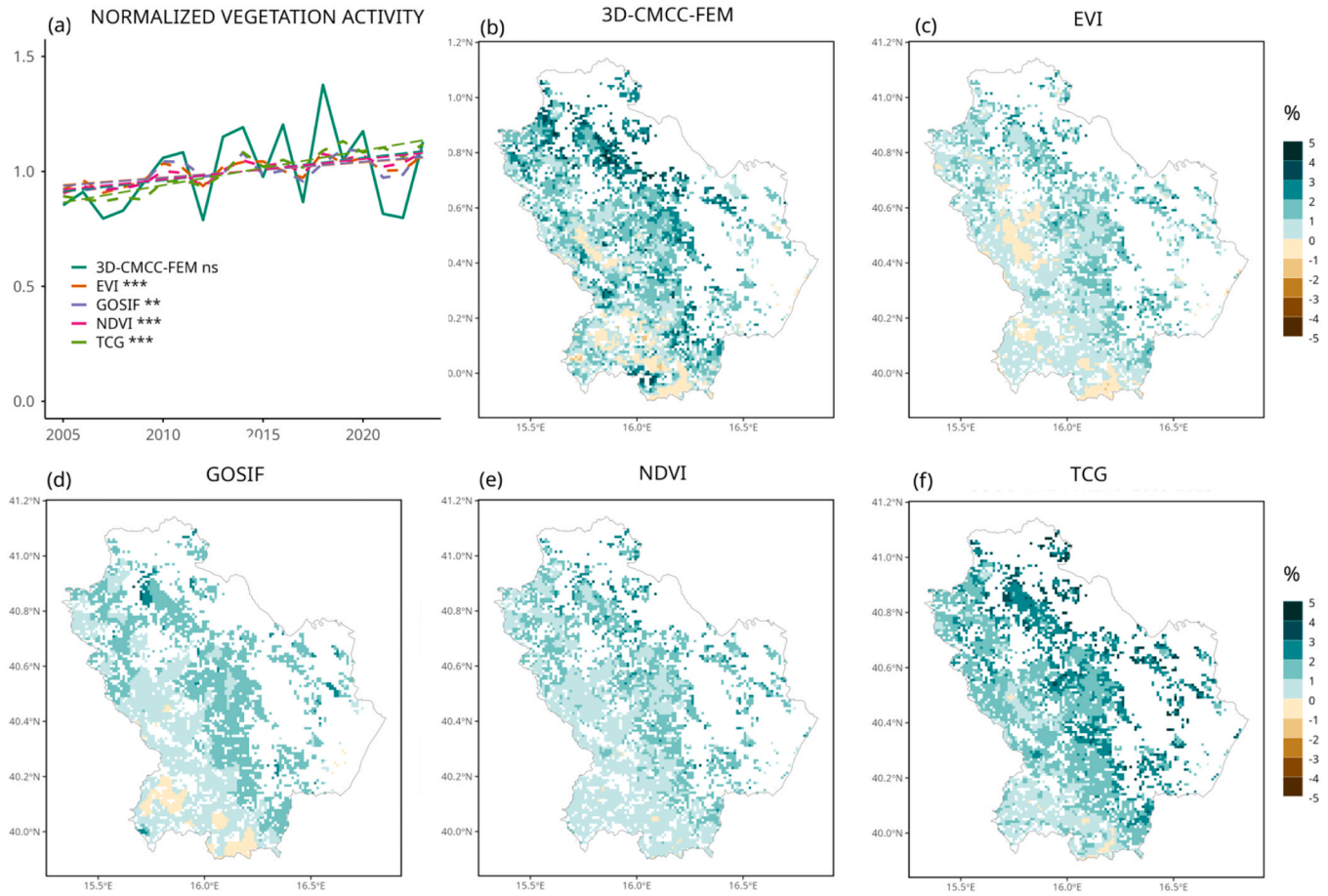

Fig. 2. a) Time series of normalized vegetation activity during the summer months (June to August); linear trend slope significance is reported as *ns*= not significant, ** P < = 0.01,*** P < 0.001; b-f) Maps of model- and RS-based trends of vegetation activity during summer in the period 2005-2023: b) 3D-CMCC-FEM modelled GPP under the present-day scenario, c) Enhanced Vegetation Index (EVI), d) Normalized Difference Vegetation Index (NDVI), e) Tasselled Cap Greenness (TCG), and c) the GOSIF-GPP dataset. Trends are reported as percentage change over the mean. White grid cells represent areas without forests (according to the NFI definition), areas not simulated by the model due a to lack of species parameterization, and areas affected by fires.

3. Results

3.1. Model simulations and comparison to satellite data

Normalized time series of summer GPP as simulated by the 3D-CMCC-FEM together with RS-based vegetation activity time series, are reported in Fig. 2a, along with the linear trend and slope significance. Interannual variability in vegetation activity well correlates among datasets. It follows the pattern of climate variability depicted by the $SPEI_{12}$ index in Fig. 1b, with apparent drops in activity in 2012, 2017 and 2022. Although generally consistent with RS-based observations, the 3D-CMCC-FEM exhibits larger negative anomalies compared to RS data. As a result, the modeled long-term GPP trend is positive but not statistically significant, in contrast to the trends derived from remote sensing. Fig. 2b-f show maps of normalized modelled GPP trends alongside RS-based estimates. Both simulated GPP and RS-based vegetation activity display a consistent and coherent spatial pattern characterized by positive trends in the southern-western part of the region (predominantly covered by *Quercus cerris* and *Quercus ilex*, Figure S1), and by lower values, or even negative trends, at the highest elevations (above 1000–1200 m), largely dominated by beech stands (Figure S1). Moving from west to east, from the Apennine range toward the plain and drier areas, decadal trend values decrease in magnitude. Among RS-based records, spatially modelled GPP trends more closely mirror the pattern estimated from the EVI and GOSIF-GPP time series. Differently from EVI and GOSIF-GPP records, TCG and NDVI-based maps show systematically positive trends in the entire region (Fig. 2d-e and Fig. 2f). Overall, all datasets indicate a positive summer greening trend; RS-based products, particularly EVI and GOSIF-GPP, show narrower, more peaked distributions, compared to the broader distribution produced by the 3D-CMCC-FEM, whose median trend is slightly higher, reflecting greater simulated variability across the simulation domain (Fig. 3). Nevertheless, the model can capture the negative trends shown by EVI and GOSIF-GPP.

When trend significance is considered, trends values provided by RS-data, i.e. EVI and GOSIF-GPP, are statistically significant in at least half of the considered simulation grid cells, where positive trends occur (Fig. 4a and S3). Modelled trends are instead mostly positive, but not significant over large areas dominated by deciduous oaks, chestnuts and Aleppo pine (Fig. 4b). Statistically significant negative trends based on the EVI-record are localized at the highest elevation over the Apennine range, covered by high forests of beech (Figure S1a). Although the model also shows negative trends in these areas, that align with EVI and GOSIF-GPP estimates, these are not, however, statistically significant (Fig. 4a-b and S3). Larger differences between EVI and GOSIF-GPP are observed when the signal is extended from March through August (Figure S4).

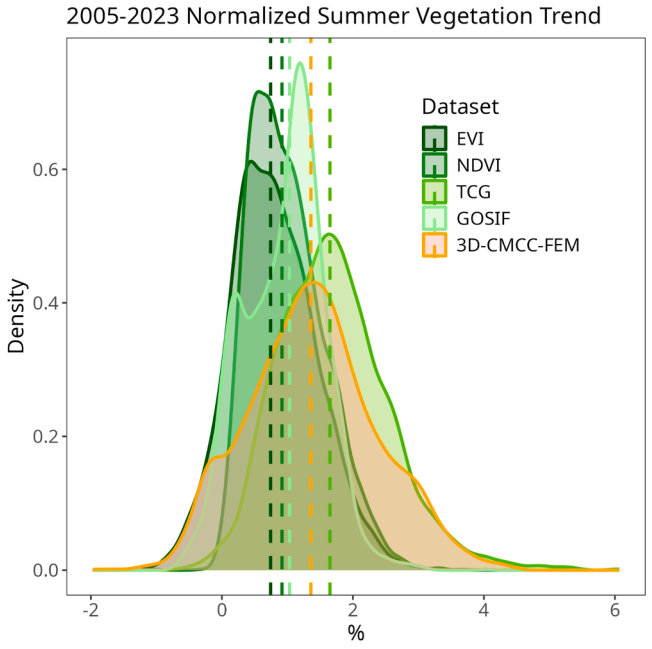

Fig. 3. Probability density functions of normalized vegetation activity trends during summer, as simulated by the 3D-CMCC-FEM model and derived from RS-based estimates: Enhanced Vegetation Index (EVI), Normalized Difference Vegetation Index (NDVI), e) Tasselled Cap Greenness (TCG), and the GOSIF-GPP dataset. Dashed lines represent the medians value.

The SPAEF metric ranges between 0.42 and 0.61, with the highest value obtained when model results are compared against EVI estimates. This holds across all SPAEF sub-metric (Table 1), with *gamma*, *beta* and *r* value of 0.92, 0.86 and 0.64 respectively. The lowest spatial variability correspondence, identified by the metric *gamma*, is found when the model is compared against TCG dataset. Generally, the relatively high *gamma* value reflects the overlapping degree across probability density functions shown in Fig. 3.

When modelled GPP and GOSIF-GPP estimates are considered in more detail, representing the same variable, the two datasets show comparable variability (see section S3 and Figure. S5) and satisfactory model performance in terms of spatial patterns and across different temporal scales (i.e. seasonal and interannual Table S2). Compared to a previous regional application (i.e., Dalmonech et al., 2024), where 3D-CMCC-FEM was forced with a different meteorological driver, performance generally improved, likely due to a more accurate representation of the precipitation field in the meteorological input.

Model performances at interannual timescales show regionally average correlation values of 0.68 and 0.56 for annual and summer anomalies, respectively (Table S1); average fractional variance values, i.e., normalized difference in variance between model and estimates of the GPP anomalies, are closer to 1. Modelled Carbon Use Efficiency values, being CUE = 1 – (Plant respiration/GPP), vary between 0.3 and 0.45 (Figure S1c), well within the range provided in literature from observations and ground data estimates (Collalti et al., 2020; Collalti and Prentice, 2019; Luo et al., 2025), confirming that the forest model maintains a realistic balanced in terms of carbon assimilation and biomass respiration (and net primary productivity). Simulated multi-year average GPP values and BAI values reflect the aboveground forest structures and productivity, with the highest GPP values occur at the highest elevation, dominated by mature beech forest and decrease toward lower elevation and plain areas mostly covered by Mediterranean pines (Figures. S1a-b and S2). Higher BAI values are simulated for mature and old-growth forests, such as those dominated by large chestnut trees (~25 cm^2), followed by black pine plantations (~40 cm^2). Lower BAI values are found in the sub-Apennine areas, where deciduous oaks form mostly young stands with coppice structure (~16 cm^2) and beech-dominated high forests (~7 cm^2). Modelled carbon stocks aggregated by forest class are comparable to estimates from the third Italian Forest Inventory (INFc, 2021) as shown in Figure S5, with the exception of *Quercus ilex*, for which the model likely overestimates tree growth.

3.2. Decadal climate impact on the GPP-BAI trends

The absolute differences in simulated trends of summer GPP and BAI between the present-day and baseline scenarios are reported in Figs. 5a and 5b, respectively. The spatial patterns of long-term trend differences are similar for both carbon assimilation and tree growth. Differences are negative in the plain areas below 200 m and in the south-western part of the region, particularly within the 500–1000 m elevation belt where trends are generally larger under the baseline scenario (i.e. larger negative differences between runs).

While both GPP and BAI trends are negatively affected by climate variability under present-day scenario across large areas, Fig. 6 shows

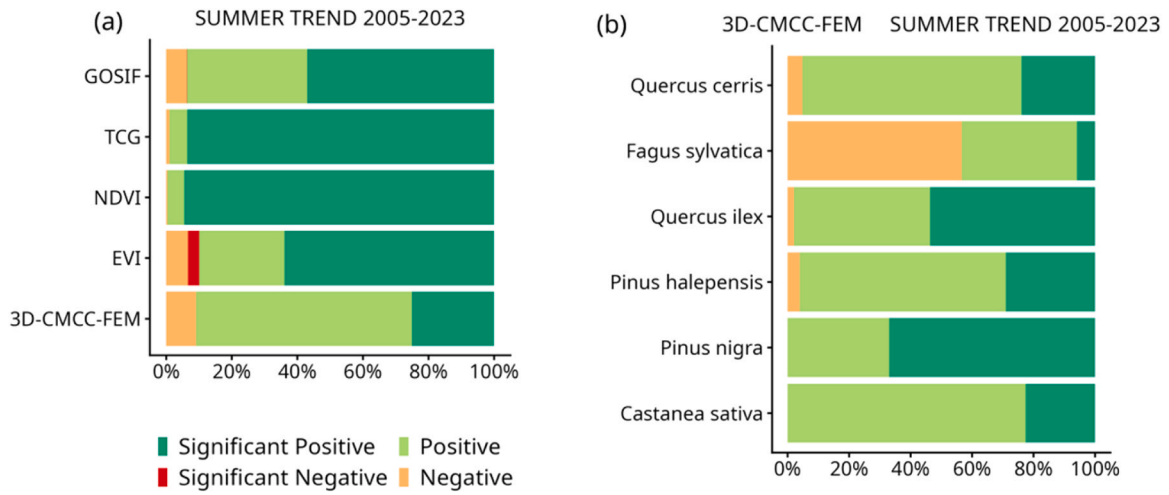

Fig. 4. a) Occurrence of positive and negative trends in summer GPP, expressed as a percentage of the total number of the simulation grid cells. Trends are computed for modelled GPP under the present-day scenario, and for RS-based vegetation activity data. Significance is assessed at $P < 0.05$. b) Occurrence of positive and negative trends in the modeled summer GPP by forest class.

Table 1
Model evaluation based on the spatial efficiency metric SPAEF for summer vegetation trends. SPAEF combines three sub-metrics: histogram overlap between observed and modelled pattern (*gamma)*, ratio of coefficient of variation, representing spatial variability (*beta)* and the spatial correlation (*r)*.

MODEL versus	SPAEF	*gamma*	*beta*	*r*
EVI	0.61	0.92	0.86	0.64
NDVI	0.53	0.87	1.27	0.63
TCG	0.42	0.92	1.44	0.63
GOSIF-GPP	0.50	0.86	1.11	0.53

that BAI-GPP coupling strength is reduced under present-day scenario, i.e. BAI responds proportionally less than summer GPP. This is reflected in the positive coupling shift shown in Fig. 6, indicating decoupling as defined in 2.5. In some areas of the region, a strong decoupling occurs, such that summer GPP and BAI show diverging trends. This is illustrated in Fig. 7, where he sign between GPP and BAI trends is mapped by aggregating results into four classes labelled as GPP^{pos}-BAI^{pos}, GPP^{pos}-BAI^{neg}, GPP^{neg}-BAI^{pos}, and GPP^{neg}-BAI^{neg} where superscripts indicate the sign of the trend (Figs. 7a and 7b). Under the baseline scenario, and across most of the simulated areas, growth patterns closely mirrored those of GPP (Fig. 7a), highlighting coupling between carbon assimilation and biomass accumulation. An exception occurs in the southern-western part of the region, within the middle-to-low-elevation forest belt, where GPP trends are mainly positive, while BAI trends are negative (Fig. 7a). The change in forested area falling into each GPP-BAI trend classes in the present-day scenario compared the baseline scenario is reported in Table 2.

Under the present-day scenario, the percentage of forest in the class GPP^{pos}-BAI^{pos}, is ~65% of the total cover, with a decrease of −25.7% compared to the baseline scenario (Table 2). The change is mirrored by a corresponding net increase in forested areas in the classes GPP^{pos}-BAI^{neg}, GPP^{neg}-BAI^{pos} and GPP^{neg}-BAI^{neg}, i.e. + 13.11%, + 7.15% + 5.47% respectively (Table 2). Modelled results indicate that the forest cover characterized by positive trends of GPP and negative trends of BAI under

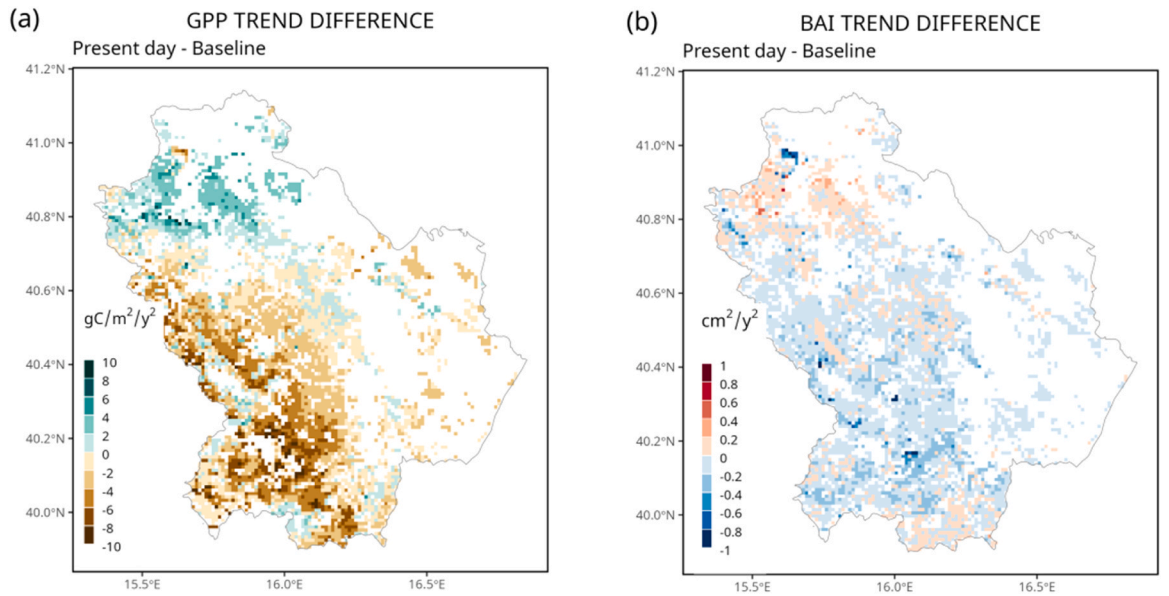

Fig. 5. Absolute differences in summer GPP and BAI trends for the 2005-2023 period between the present-day and baseline scenarios. White grid cells represent areas without forests (according to the NFI definition), areas not simulated by the model due to a lack of species parameterization, and areas affected by fires.

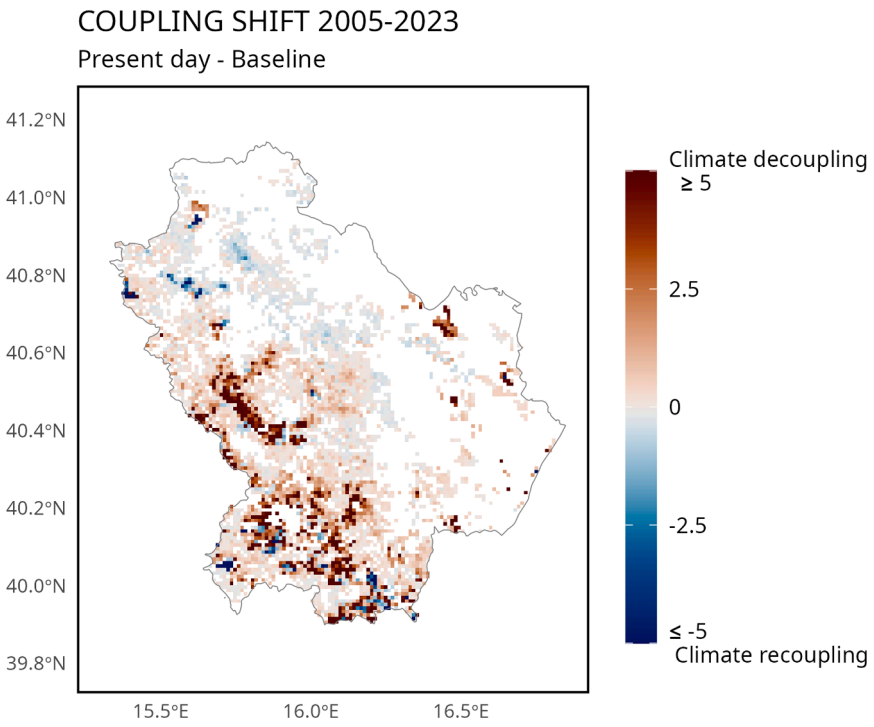

Fig. 6. Coupling shift of the BAI-GPP association strenght, computed as differences between the elasticity metric computed under present-day and baseline scenarios. Positive differences indicate "decoupling", i.e. BAI respond less than GPP under the present day, and negative differences indicate, indicate 'recoupling', i.e. strengthens of the coupling. White grid cells represent areas without forests (according to the NFI definition), areas not simulated by the model due a to lack of species parameterization, and areas affected by fires.

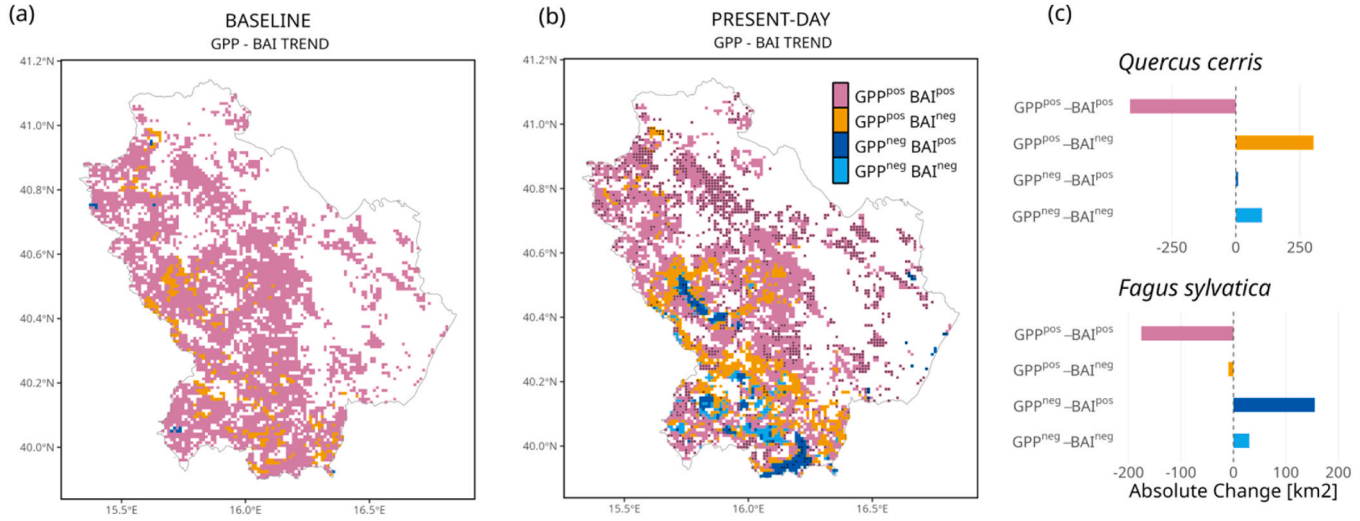

Fig. 7. Occurrence of positive and negative trends in summer GPP and BAI, classified by sign association into four classes: GPP^{pos}-BAI^{pos}, GPP^{pos}-BAI^{neg}, GPP^{neg}-BAI^{pos}, and GPP^{neg}-BAI^{neg} where superscripts indicate the sign of the trend, under a) baseline and b) present-day scenario. Areas where BAI trends under present-day scenario are significant ($P < 0.05$) are indicated by hatching. White grid cells represent areas without forests (according to the NFI definition), areas not simulated by the model due a to lack of species parameterization, and areas affected by fires. c) Net change in forest cover between the present-day and baseline scenario within the four GPP-BAI classes reported for areas dominated by *Q. cerris* and *F. sylvatica*.

the present-day scenario is ~21%. A qualitative similar result is also observed when extending the GPP signal to the full growing season (Figure S8), with a net increase in forested areas described by opposite GPP-BAI trends.

When considering forest classes, about 68% of deciduous oak forests currently fall into the class GPP^{pos}-BAI^{pos}, and 25.3% in GPP^{pos}-BAI^{neg} class (Table 2), the latter mostly located in the low hilly bioclimatic belt up to about 1000 m (Figure S8). Compared to the baseline scenario, deciduous oak forests show a net loss of area in the class GPP^{pos}-BAI^{pos} of −23.7%, corresponding to ~ 400 km^2.The net change is mirrored by an increase of a + 17.4% in the GPP^{pos}-BAI^{neg} class, ~ 300 km^2, (Fig. 5c), and + 5.8% increase of areas in the GPP^{neg} -BAI^{neg} class, ~ 100 km^2 (Fig. 7c, Table 2).

In beech-dominated forests under present-day scenario, the model shows as only 18.1% of areas are characterized by positive trends of both GPP and BAI. The majority, 54.3%, belong to the class GPP^{neg}-BAI^{pos} principally occurring at high elevations, in the range of 1100–1800 m (Table 2 and Figure S9) and 17.1% to the class GPP^{pos}-BAI^{neg}. The

Table 2
Forest cover change within each GPP-BAI association class between the present-day and baseline scenarios. Data are expressed as percentage by forest class defined as forested areas dominated by a single species. GPP data refer to summer months (June to August). For each forest class, the values in brackets indicate the percentage of forest cover falling within each GPP-BAI association class under the present-day scenario.

GPP-BAI Class	Forest Class						
	All	***Quercus cerris***	***Fagus sylvatica***	***Castanea sativa***	***Quercus ilex***	***Pinus nigra***	***Pinus halepensis***
GPP^{pos}-BAI^{pos}	-25.74 (65.2)	-23.7 (68.0)	-59.7 (18.1)	-25.0 (63.0)	-2.4 (97.6)	-1.3.8 (98.7)	-6.6 (93.4)
GPP^{pos}-BAI^{neg}	13.11 (21.7)	17.4 (25.3)	-3.3 (17.1)	25.0 (37.0)	0.0 (0.0)	1.3 (1.3)	1.8 (1.8)
GPP^{neg}-BAI^{pos}	7.15 (7.5)	0.5 (0.8)	52.7.3 (54.3)	0.0 (0.0)	2.4 (2.4)	0.0 (0.0)	4.8 (4.8)
GPP^{neg}-BAI^{neg}	5.47 (5.4)	5.8 (5.8)	10.3 (10.3)	0.0 (0.0)	0.0 (0.0)	0.0 (0.0)	0.0 (0.0)

remaining beech forests, namely 10.2%, are in the class GPP^{neg}-BAI^{neg} and are mostly located in the low-elevation range (Figure S8). Similarly to oak dominated areas, beech forests also show a net change of area from the class GPP^{pos}-BAI^{pos}, −59.7% corresponding to ~ 170 km^2.(Fig. 7c). This change principally reflects an increase of areas described by negative summer GPP with positive trends in BAI, + 52.7% corresponding to ~ 155 km^2 (Fig. 7c).

Results for the remaining forest classes, that altogether cover about 6.9% of the total forested area of the region, are reported in Table 2 only. Model results indicate relatively minor changes in the frequency of GPP–BAI classes. Holm oak and black pine exhibit net changes of approximately 1–2%, while Aleppo pine shows a net change of ~-6% in the GPP^{pos}-BAI^{pos} class. However, only a few and sporadic grid cells are affected. Chestnut forests display a more pronounced decrease, with a 25.0% reduction in the GPP^{pos}-BAI^{pos} association class. While the four GPP-BAI classes shown in Fig. 7 are spatially robustly localized, the statistical significance of the negative trends for the long-term trend BAI is very sporadic, yet it occurs in beech-dominated forests and in the north-eastern part of the region.

3.3. BAI trend spatial pattern

The Random Forest algorithm was used to rank the importance of the selected predictors in statistically explaining the simulated spatial pattern of BAI trends. The model embedding structural variables, soil-related variables, and using SPEI as the climate-related driver alone explained about 82% of the BAI trend variability (Fig. 8 inset). All the predictors are statistically significant in explaining the spatial variability of BAI. Initial stand density was the most important explanatory factor, followed by GPP during spring and summer, age class, average $SPEI_{12}$ values during spring, and average initial DBH (Fig. 8).

Fig. 8b–d shows the partial dependence plots for the three most important variables, illustrating a monotonic decreasing relationship between BAI trend and initial stand density, while a less clear pattern is revealed when considering GPP in spring and summer. Compared to other statistical methods, Random Forest automatically handles non-linearity and interactions among covariates (Breiman, 2001). However, the similar increases in MSE across the remaining variables beyond the top-ranked one suggest a reduced ability to clearly distinguish the relative contribution of individual predictors, potentially reflecting the presence of multicollinearity among explanatory variables.

Predictor rankings were largely unchanged when meteorological variables were explicitly included (Figure S10). Stand density remained the most important explanatory variable; however, more relevance in the ranking is given to the precipitation signal during summer and soil depth.

The RF model showed a weak spatial autocorrelation of 0.09 in its residuals (Moran's I = 0.002, P < 0.001), close to zero, indicating that the spatial structure in the response variable was effectively captured by the included predictors. Consequently, residuals are approximately spatially uncorrelated. Model performance and predictor rankings were largely unaffected by addition of spatial covariates (latitude and longitude; Table S3, Figure S11).

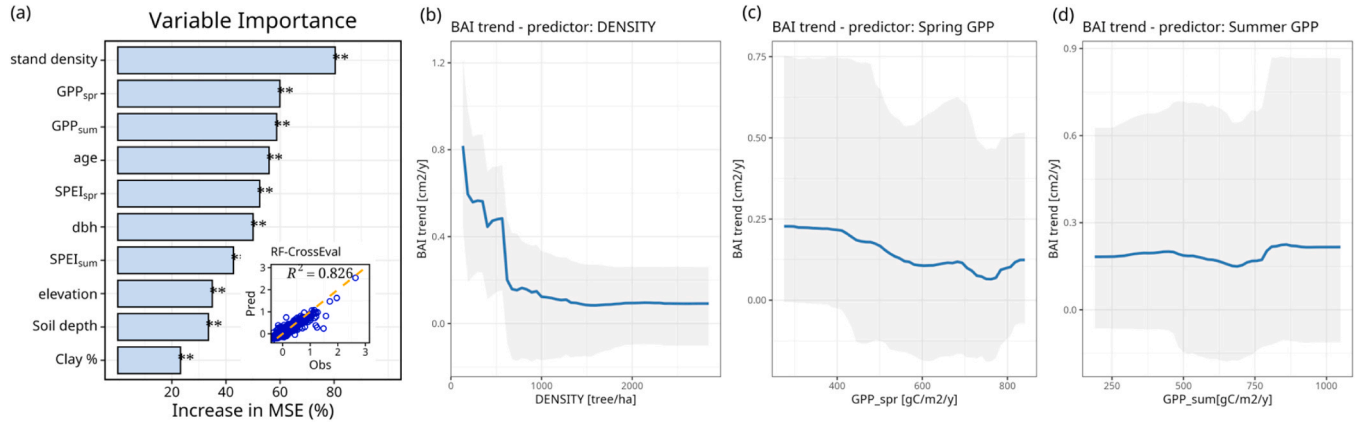

Fig. 8. a) Variable importance in explaining spatial patterns of BAI trends according to the Random Forest (RF) algorithm (number of trees=1000, training on the 70% of the data, cross-evaluation on the 30%). Importance is reported as increase in the mean squared error, MSE, with permutation testing for significance (* P < 0.05** P < 0.01). Inset: cross-evaluation result of the Random Forest model, R^2 coefficient of determination; b-d) partial dependence plots for the three most influential predictors of BAI trends, b) Stand density, c) spring GPP, c) summer GPP. Partial dependence plots report confidence interval at 95%, blue line is the average predicted value. The list of predictors include: stand density, average stand age class (age), average stand diameter at breast height (dbh), cumulative GPP in summer (GPP_{sum}), cumulative GPP value in spring (GPP_{spr}), elevation, soil depth and soil percentage of clay (Clay %).

4. Discussions

Climate change does not affect all components of forest ecosystems uniformly or synchronously: responses frequently differ in both magnitude and timing across ecosystem compartments (Kannenberg et al., 2020), a pattern particularly pronounced in Mediterranean regions (e.g. Nolè et al., 2013). In this study, we investigate the long-term effects of climate variability over the past two decades on forest functioning in a Mediterranean area of southern Italy. We adopt a factorial modelling approach to separate intrinsic biological trends from the effects of decadal climate variability. Using a state-of-the-art mechanistic forest model, we provide an ecosystem-level, broad-scale perspective on how key processes, such as seasonal carbon assimilation and tree growth, have responded to changing climatic conditions, highlighting potential shifts in productivity patterns, forest resilience, and ecosystem carbon dynamics.

4.1. How does climate variability influence decadal carbon processes and tree dynamics in Mediterranean forests?

Modelled results indicate that recurrent droughts over the past two decades have exerted a sustained negative effect on both seasonal carbon assimilation trends and tree growth, with growth trends likely being more strongly impacted. Despite this negative climate impact, both the 3D-CMCC-FEM results and independent RS-datasets show a coherent spatial pattern, characterized by a general summer greening across the most of the study region, which is statistically significant in the observational records. The observed positive trends in GPP are consistent with the "CO_2 fertilization effect" hypothesis (Gonsamo et al., 2021; Zhu et al., 2016), which is explicitly represented in the 3D-CMCC-FEM model. This hypothesis suggests that rising atmospheric CO_2 concentrations can enhance plant photosynthesis, potentially stimulating forest gross productivity. At the same time, forest management practices contribute to landscape heterogeneity, further modulating these productivity patterns, which are by design simulated in the model. Indeed, forest inventory data estimates show the occurrence of relatively young forest in the Mediterranean compared to e.g., central Europe, a condition arising from both natural and anthropogenic drivers, with large areas managed as coppice (INFc, 2021). The high frequency of stand in young age classes, typically indicated to show a higher CO_2 fertilization effects (e.g. Collalti et al., 2018; Norby et al., 2016) and the natural stand development before fully canopy closure, likely contribute to the observed positive vegetation activity trends. Under these conditions, increases in growth, are very well known to be associated with positive trends following stand development, hence trends of carbon assimilation and tree-level growth are expected to align. Yet, it has also been shown, how even mature forest with large trees might still show sustained growth and positive BAI trends (e.g. Fekedulegn et al., 2003; Stephenson et al., 2014).

Interestingly, our model-based results also highlight an emerging large-scale pattern, where a climate-induced decoupling of BAI and GPP association strength occurs and specific areas in the region show even a divergent trend in seasonal carbon assimilation and growth. This divergence is already occurring under the baseline scenarios in some areas, yet amplified under present-day climate, with a greater proportion of forested areas affected.

The rate of decoupling between carbon assimilation and growth remains a longstanding topic of debate (Boukhris et al., 2025). Scientific evidence indicates that photosynthesis and diametric growth can become decoupled over short (monthly) to annual timescales (Anderson-Teixeira and Kannenberg, 2022; Cabon et al., 2022; Martínez-Sancho et al., 2022) Other studies have shown that, at annual scales, tree-ring chronologies and remote sensing-based proxies of vegetation activity tend to be closely correlated across forests in Spain and southern Italy, although the strength of these correlations may vary with species and edaphic conditions (Castellaneta et al., 2022; Vicente-Serrano et al., 2020). Differently, the present study reveals a long-term decoupling and diverging pattern of assimilation and growth emerging at decadal scales, suggesting that recurrent drought stress could reduce growth independently by the apparent long-term positive trend of photosynthetic activity, as also suggested in Lempereur et al. (2015).

Our modelling results of a general growth decline are also supported by local observations of growth decline in deciduous oak sites. Following recent droughts and heat waves, several deciduous oak-dominated stands in the regions have experienced dieback events, with healthy and weakened trees coexisting within the same site (see Colangelo et al., 2017; Conte et al., 2025). In addition, the identified hotspot areas of GPP-BAI decoupling approximately mirror the vulnerability maps presented in Conte et al. (2025), based on recurrency of defoliation events in deciduous oak stands in the region between 2015 and 2022.

Previous studies have suggested that dry conditions might explain the decoupling of the C-source and -sink, i.e., the tree-ring with a GPP-based signal observed on-site (e.g. Cabon et al., 2022). In this context, during the summer, stomatal closure may limit carbon assimilation by trees as response to drought (Gessler et al., 2018). Nevertheless, carbon reserves generally remain sufficient to sustain metabolic functions under conditions of limited carbon supply, albeit at the expense of stem growth as indicated in Huang et al. (2021), which can, in turn, influence carbon allocation patterns in subsequent years as suggested in Peltier and Ogle (2019). This imbalance in carbon allocation, actively regulated by the carbon reserve pool (Gessler and Zweifel, 2024), might loop back on growth over longer temporal scales and under frequent drought events as suggested by our modelling results. Indeed, Anderegg et al. (2015), demonstrated a prevalent drought legacy on growth, particularly in dry ecosystems. Trees rely on reserves to recover from hydraulic damage, such as embolism, and to maintain metabolic functions under stress (Hammond et al., 2022). However, if unfavourable conditions persist, repeated or prolonged reserve consumption can trigger long-term negative feedback: reduced carbon availability limits stem growth and other allocation pathways (e.g., to leaves), weakening overall tree vigour. Under prolonged and intense drought both growth and carbon reserved have shown to decline in a Mediterranean woody species (Rosas et al., 2013) and *Fagus sylvatica* forests subjected to rain exclusion in France (Chuste et al., 2020).

Peltier et al. (2024) showed that trees in drier sites in the US experience elevated Non-Structural Carbohydrate (NSC), i.e. carbon reserve, consumption and reduced mixing in the sapwood under prolonged dry conditions, because very likely photosynthesis can stop but not plant respiration. This cascading effect can ultimately reduce stand-level resilience and carbon use efficiency, increasing tree vulnerability to subsequent stress events (Collalti et al., 2020; He et al., 2020; Peltier et al., 2023). The modelled decoupling between seasonal carbon assimilation and average tree growth, while broadly consistent with mechanistic and physiologial explanation outlined above, is not systematic across the entire Mediterranean region under study; diverging trajectories are also shaped by other biotic and abiotic factors, beyond external climate forcing, as indicated in the next section.

4.2. How forest structure and species shape the climate induced divergence of sink and source?

Our modelling results show how a general long-term greening over the entire region under study, might mask a negative trend of tree growth, a precursor for the loss of resilience capacity, hence in turn increased vulnerability and tree mortality risk (Cailleret et al., 2017; Neycken et al., 2022; Pedersen, 1998). This pattern of negative and diverging trends holds particularly for deciduous oaks and beech dominated forests at the lower elevations. Among the other forest classes, the positive trends of both carbon assimilation and tree growth in forests dominated by holm oaks reflect the capacity of several evergreen oak species to withstand periods of drought (Heinrich et al.,

2025). Similarly, among pine species, Aleppo pine has been shown to have high plasticity and drought tolerance resulting in a wide geographical distribution in the Mediterranean, although a reduced growth was observed in the drier areas of its distribution following severe drought events (Dorman et al., 2015; Gazol et al., 2017).

Notably, the 3D-CMCC-FEM shows a tendency for GPP and growth trends to diverge even under the baseline scenarios, indicating that site legacy,primarily reflected in the forest structure estimated for 2005, plays a critical role in shaping forest dynamics under a changing climate (Astigarraga et al., 2025; Petritan et al., 2021). Incorporating current ground-based forest observations, such as stand density, as model initial conditions allows legacy effects on growth to be explicitly represented (Kannenberg et al., 2020; Vayreda et al., 2012). Accounting for these legacy effects has proven critical for accurately assessing drought-induced mortality risk (Sterck et al., 2024). For instance, highly dense forests show slower growth compared to less dense forests, a trend that can be exacerbated under drought conditions and soil moisture scarcity (Rubio-Cuadrado et al., 2018).

Beyond stand density, other structural forest characteristics such as stand age and size (i.e. DBH as proxy of the amount of biomass) modulate the forest's sensitivity to climate variability, as indicated in our study. Higher-elevation forests are dominated by older age classes and larger trees, with individual tree growth remaining positive, as also recently observed in the Balkan region (Markuljaková et al., 2026). These observations align with recent studies indicating that old forests can maintain, under current climate conditions, high resistance and potentially resilience under both Mediterranean and temperate climates (Colangelo et al., 2021; Puchi et al., 2024). Although larger trees are theoretically and empirically associated with higher respiration costs (Collalti et al., 2020), their size also corresponds to greater carbon reserve pools. This holds for instance for European beech, a diffuse-porous ring species, which in our modelling results shows no negative BAI trends at higher elevations despite negative trends in the summer carbon assimilation and vegetation activity. Mature stands composed by bigger trees might have larger pools of carbon reserve and the ability to buffer year-to-year climate anomalies impacts more efficiently as suggested in Zweifel and Sterck (2018). However, to this respect, the modelled tree ability to buffer climate extremes impact depends not only on the carbon reserve pool size but also on species-specific physiological traits and edaphic conditions, making drought impact non-uniform across species.

At medium to high elevations, beech trees may be more energy-limited and could therefore benefit from increased carbon assimilation during warmer springs or earlier snowmelt (Nezval et al., 2025; Signarbieux et al., 2017), potentially advancing the onset of wood enlargement ahead of summer heat stress (Grossiord et al., 2022). Notably, however, modelled tree growth trends appear decoupled from the negative summer GPP trends indicated by both the model and several remote sensing products. At lower elevations, beech stands tend to show a growth decline. Enhanced vegetation activity during the spring might likely amplify the drought impact as transpiration occurs at higher rates, potentially decreasing soil water availability later into the year (Bastos et al., 2021), contributing to declining carbon assimilation at the end of the spring season, and in turn, to reserve depletion and growth reduction (Bose et al., 2025). This pattern, differently from results in Martinez del Castillo et al. (2022), suggests a substantially more heterogeneous response in beech-dominated forests.

At the national level, it has been shown that in the period 2010–2022, beech-dominated sites experienced an increasing rate of defoliation, which was, however, not accompanied by a significant increase in tree mortality; conversely deciduous oaks, i.e., *Quercus cerris*, showed a significant increase in mortality rates (ICP-forest monitoring network plots; Bussotti et al., 2024).

Compared to beech, deciduous oaks have ring-porous anatomy, hence, a small amount of active tree ring and sapwood, the latter a variable which is prognostically simulated in the 3D-CMCC-FEM. Therefore, oaks might respond more tightly to the current-year drought event, with long-term impacts (Zweifel and Sterck, 2018). In oak forests in the dry-subhumid areas of the study region, a persistent combination of low water resource availability and declining growth may deplete carbon reserves, impairing the capacity to sustain metabolic processes and repair potential hydraulic damage, despite oaks being known to be drought-tolerant species. This dynamic can increase tree vulnerability, potentially leading to higher mortality risk and reduced stand resilience under expected increase in recurrent drought events in the near future (Desprez-Loustau et al., 2006; Gentilesca et al., 2017; Piper et al., 2022;, Gazol et al.2020).

4.3. Study limitations and challenges

Despite the robustness of the 3D-CMCC-FEM model, some sources of uncertainty in model performance and process representation required further discussion and clarification. As with all process-based, mechanistic models, simulated outputs are emergent properties arising from internal feedbacks rather than being explicitly prescribed; they cannot therefore be systematically tested against observations, and the dynamics of key variables, such as carbon reserve, are particularly difficult to evaluate in regions like the Mediterranean, where experimental data are fragmented in space and time. However, the mechanistic nature of the model ensures a fully consistent and unbiased representation of carbon dynamics: consistency is guaranteed by the closed mass balance, prescribed initial conditions close to observations, and tightly constrained parameters and simulations. For these reasons, we expect that the modelled trajectories of seasonal carbon assimilation and growth, to be coherently modulated by carbon reserves dynamics. Future long-term experimental studies aiming at simulating recurrent drought impacts should monitor all the three components of the tree carbon dynamics, namely photosynthesis, growth and carbon reserve, to provide compelling evidence of the identified long-term assimilation-growth decoupling.

To keep simulations feasible and constrain the number of simulations, a simplified setup was used to initialize the model, which also had to align with the details of the soil and climate inputs, the latter still provided at a relatively coarse resolution. Model simulations do not account for any shifts in stand species composition that may have occurred over the 18-year study period, and therefore cannot capture the potential establishment of more drought-tolerant tree species. The 3D-CMCC-FEM uses physiological, species-specific parameters that are, however, general and not locally calibrated, which might partially explain the lower occurrence of statistically significant trends compared to RS-based data. Similarly the lack of significance in the modelled trends might be the result of the high model responsiveness to summer precipitation shortage, a behaviour previously reported for other models (e.g. 3-PG; Nolè et al., 2013) and for the 3D-CMCC-FEM model and attributed to the parsimonious representation of soil water dynamics (Saponaro et al., 2025). This in turn makes the results more sensitive on the choice of the forcing dataset of precipitation field.

In this study, ERA-5 Land was selected as of one of the state-of-the-art global meteorological dataset. In Italy, ERA5-Land was shown already to be a valuable product for monitoring hydrological variables in agricultural contexts (Vanella et al., 2022), outperforming satellite based gridded datasets of precipitation (Moccia et al., 2025). Uncertainties remain in the representation of summer convective precipitation events in southern Italy, a limitation common to other reanalysis product (Cavalleri et al., 2024, Raffa et al., 2021). Other gridded datasets based on ground observations exist, such as E-OBS (Cornes et al., 2018). However its sparse station coverage in the study region leads to higher uncertainty in the precipitation field. Forcing the forest model with E-OBS yielded similar "hotspot" maps (Fig. 7 and Figure. S13), with a stronger climate impact on tree growth, as result of a likely underestimation of summer precipitation.

Other potential extremes affecting Mediterranean forests are

missing, such as frost events (D'Andrea et al., 2021). However, the effect of frost is currently not included in the model, and it would require highly accurate daily meteorological data to simulate its impact. Similarly, the model has been developed to run offline at daily time scales, with readily available meteorological drivers. Therefore, it does not simulate sub-daily processes, particularly finer mechanisms of the plant hydraulic system, which might lead to sudden mortality events without growth decline (Gessler et al., 2018). However the 3D-CMCC-FEM rather aims to capture the average stand behaviour and the long-term quasi-active role of carbon reserves in influencing the allocation of newly assimilated carbon, e.g., toward assimilation rather than growth (Gessler and Zweifel, 2024), and despite the aforementioned uncertainties, we show that the model provides consistent, explainable temporal and spatial trends of GPP and BAI.

The role played by the initial stand structure is prominent: the persistence of long-term GPP-growth trend divergence does not significantly differ in terms of spatial extent and location of affected forested areas when the model is driven with a different forcing dataset (Figure. S12).

However, different climate forcing might shift the timing of divergence and strengthen trends. Improvement in the spatial resolution and accuracy of meteorological datasets will directly enhance the fidelity of simulated carbon dynamics. However, such gains can only be fully realized if the resolution of climate inputs is matched by an equivalent level of detail in forest structural characterization. Hence, the needed accuracy of the initial forest structure and climate data to constrains future forest dynamics trajectories in time and space, put emphasis on initiatives such as the *Global Ecosystem Dynamics Investigation* (*GEDI,* Duncanson et al., 2022), or climate impact research initiative such as ISIMIP (Frieler et al., 2024), providing high resolution climate data and climate projections (Malle et al., 2025).

5. Conclusions

This study offers a comprehensive picture of how a Mediterranean forest in southern Italy functions under recent climate change in southern Italy, accounting for multiple drivers of long-term association and decoupling between carbon assimilation and tree growth, eventually leading to growth decline. We identify how and to what extent decadal climate variability in a Mediterranean region affected trends in carbon assimilation and tree woody growth, pinpointing areas that already show a background growth decline, often masked by long-term canopy-level greening. The reconstructed forest dynamics across representative Mediterranean stands revealed emerging, large-scale and divergent trajectories of carbon assimilation and tree growth, shaped by structural differences, species-specific eco-physiology, and climate variability impacts over the last two decades.

Even in the absence of an evident, visible, long-term decline in functioning, or, conversely, in the presence of an apparent decline, continuous monitoring activities in particular through mechanistically approaches as shown in this study, are shown to be critical to investigate how canopy level functioning translates into tree growth. Monitoring activity, informed by knowledge of actual forest structure and, in parallel, by accurate climate data, are pivotal for optimizing target management and the effectiveness of restoration measures.

Author contribution

D.D. conceived the study, designed and performed the model simulations. D.D. and E.V-. analyzed the data. E.V. and Q.D. were responsible for data curation. A.C. was responsible for software and funding acquisition. All co-authors contributed to the discussion of the results and the review and editing of the manuscript.

CRediT authorship contribution statement

Daniela Dalmonech: Writing – review & editing, Writing – original draft, Visualization, Validation, Methodology, Investigation, Formal analysis, Data curation, Conceptualization. **Dánnell Quesada Chacón:** Writing – review & editing, Resources, Data curation. **Elia Vangi:** Writing – review & editing, Methodology, Formal analysis, Data curation. **Alessio Collalti:** Writing – review & editing, Software, Project administration, Funding acquisition.

Declaration of Competing Interest

The authors declare that they have no known competing financial interests or personal relationships that could have appeared to influence the work reported in this paper.

Acknowledgments

This research was supported by the European Union – NextGenerationEU under the National Recovery and Resilience Plan (NRRP), Mission 4 Component 2 Investment 1.4 - Call for tender No. 3138 of December 16, 2021, rectified by Decree n.3175 of December 18, 2021, of the Italian Ministry of University and Research under award Number: Project code CN_00000033, Concession Decree No. 1034 of June 17, 2022 adopted by the Italian Ministry of University and Research, CUP B83C22002930006, Project title "National Biodiversity Future Centre – NBFC". D.Q-C. acknowledges the project TipESM "Exploring Tipping Points and Their Impacts Using Earth System Models". TipESM is funded by the European Union. Grant Agreement number: 101137673. We thank the anonymous reviewer for their constructive comments and suggestions, which helped improve the manuscript. We also thank Elisa Grieco for assistance in improving the language.

Appendix A. Supporting information

Supplementary data associated with this article can be found in the online version at doi:10.1016/j.foreco.2026.123843.

Data availability

The 3D-CMCC-FEM model code version 5.6 is publicly available under the GNU General Public Licence v3.0 (GPL) and can be found on the GitHub platform at: https://github.com/Forest-Modelling-Lab/3D-CMCC-FEM. All data, model executable, and scripts to perform analyses and figures presented in this work are provided open access in the Zenodo server (https://doi.org/10.5281/zenodo.18701467). Correspondence and requests for additional materials should be addressed to the corresponding author.

References

Anderegg, W.R., Schwalm, C., Biondi, F., Camarero, J.J., Koch, G., Litvak, M., Pacala, S., 2015. Pervasive drought legacies in forest ecosystems and their implications for carbon cycle models. Science 349 (6247), 528–532.

Anderson-Teixeira, K.J., Kannenberg, S.A., 2022. What drives forest carbon storage? The ramifications of source-sink decoupling. Source. N. Phytol. 236 (1), 5–8. https://doi.org/10.2307/27179066.

Astigarraga, J., Calatayud, J., Ruiz-Benito, P., Madrigal-González, J., Tijerín-Triviño, J., Zavala, M.A., Andivia, E., Herrero, A., 2025. Forest structural diversity modulates tree growth synchrony in response to climate change. For. Ecol. Manag. 579, 122505. https://doi.org/10.1016/j.foreco.2025.122505.

Bastos, A., Orth, R., Reichstein, M., Ciais, P., Viovy, N., Zaehle, S., Anthoni, P., Arneth, A., Gentine, P., Joetzjer, E., Lienert, S., Loughran, T., McGuire, P.C., Sungmin, O., Pongratz, J., Sitch, S., 2021. Vulnerability of European ecosystems to two compound dry and hot summers in 2018 and 2019. Earth Syst. Dyn. 12 (4), 1015–1035. https://doi.org/10.5194/esd-12-1015-2021.

Bathiany, S., Bastiaansen, R., Bastos, A., Blaschke, L., Lever, J., Loriani, S., Boers, N., 2025. Ecosystem resilience monitoring and early warning using Earth observation data: challenges and outlook. Surv. Geophys. 46 (2), 265–301.

Biondi, F., Qeadan, F., 2008. A Theory-Driven Approach to Tree-Ring Standardization: Defining the Biological Trend from Expected Basal Area Increment. Tree-Ring Res. 64 (2), 81–96. https://doi.org/10.3959/2008-6.1.

Bose, A.K., Etzold, S., Meusburger, K., Gessler, A., Baltensweiler, A., Braun, S., Buchmann, N., Camarero, J.J., Haeni, M., Kahmen, A., Peters, R.L., Sterck, F.J., Tresch, S., Walthert, L., Zweifel, R., 2025. Decreasing Stem Growth in Common European Tree Species Despite Earlier Growth Onset. Glob. Change Biol. 31 (7). https://doi.org/10.1111/gcb.70318.

Boukhris, I., Marano, G., Dalmonech, D., Valentini, R., Collalti, A., 2025. Modeling Forest Growth Under Current and Future Climate. Curr. For. Rep. 11 (1), 17. https://doi.org/10.1007/s40725-025-00249-5.

Breiman, L., 2001. Random forests. Mach. Learn. 45 (1), 5–32. https://doi.org/10.1023/A:1010933404324.

Buck, A.L., 1981. New equations for computing vapor pressure and enhancement factor. J. Appl. Meteorol. Climatol. 20 (12), 1527–1532.

Buck Research Instruments LLC, 2010. Model CR-1A hygrometer with autofill: Operating manual. ⟨http://www.hygrometers.com/wp-content/uploads/CR-1A-users-manual-2009-12.pdf⟩.

Bussotti, F., Papitto, G., Di Martino, D., Cocciufa, C., Cindolo, C., Cenni, E., Bettini, D., Iacopetti, G., Ghelardini, L., Moricca, S., Panzavolta, T., Bracalini, M., Pollastrini, M., 2024. Extreme climatic events, biotic interactions and species-specific responses drive tree crown defoliation and mortality in Italian forests. IForest - Biogeosciences For. 17 (5), 300–308. https://doi.org/10.3832/ifor4531-017.

Cabon, A., Kannenberg, S.A., Arain, A., Babst, F., Baldocchi, D., Belmecheri, S., Delpierre, N., Guerrieri, R., Maxwell, J.T., McKenzie, S., Meinzer, F.C., Moore, D.J. P., Pappas, C., Rocha, A.V., Szejner, P., Ueyama, M., Ulrich, D., Vincke, C., Voelker, S.L., Anderegg, W.R.L., 2022. Cross-biome synthesis of source versus sink limits to tree growth. Science 376 (6594), 758–761. https://doi.org/10.1126/science.abm4875.

Cailleret, M., Jansen, S., Robert, E.M.R., Desoto, L., Aakala, T., Antos, J.A., Beikircher, B., Bigler, C., Bugmann, H., Caccianiga, M., Čada, V., Camarero, J.J., Cherubini, P., Cochard, H., Coyea, M.R., Čufar, K., Das, A.J., Davi, H., Delzon, S., Martínez-Vilalta, J., 2017. A synthesis of radial growth patterns preceding tree mortality. Glob. Change Biol. 23 (4), 1675–1690. https://doi.org/10.1111/gcb.13535.

Castellaneta, M., Rita, A., Camarero, J.J., Colangelo, M., Ripullone, F., 2022. Declines in canopy greenness and tree growth are caused by combined climate extremes during drought-induced dieback. Sci. Total Environ. 813, 152666. https://doi.org/10.1016/j.scitotenv.2021.152666.

Cavalleri, F., Lussana, C., Viterbo, F., Brunetti, M., Bonanno, R., Manara, V., Maugeri, M., 2024. Multi-scale assessment of high-resolution reanalysis precipitation fields over Italy. Atmos. Res. 312, 107734.

Chapman, M., Jung, M., Leclère, D., Boettiger, C., Augustynczik, A.L.D., Gusti, M., Ringwald, L., Visconti, P., 2025. Meeting European Union biodiversity targets under future land-use demands. Nat. Ecol. Evol. 9 (5), 810–821. https://doi.org/10.1038/s41559-025-02671-1.

Chiew, F.H., 2006. Estimation of rainfall elasticity of streamflow in Australia. Hydrol. Sci. J. 51 (4), 613–625.

Chuste, P.A., Maillard, P., Bréda, N., Levillain, J., Thirion, E., Wortemann, R., Massonnet, C., 2020. Sacrificing growth and maintaining a dynamic carbohydrate storage are key processes for promoting beech survival under prolonged drought conditions. Trees 34 (2), 381–394.

Colangelo, M., Camarero, J.J., Battipaglia, G., Borghetti, M., De Micco, V., Gentilesca, T., Ripullone, F., 2017. A multi-proxy assessment of dieback causes in a Mediterranean oak species. Tree Physiol. 37 (5), 617–631. https://doi.org/10.1093/treephys/tpx002.

Colangelo, M., Camarero, J.J., Gazol, A., Piovesan, G., Borghetti, M., Baliva, M., Gentilesca, T., Rita, A., Schettino, A., Ripullone, F., 2021. Mediterranean old-growth forests exhibit resistance to climate warming. Sci. Total Environ. 801, 149684. https://doi.org/10.1016/j.scitotenv.2021.149684.

Collalti, A., Prentice, I.C., 2019. Is NPP proportional to GPP? Waring's hypothesis 20 years on. Tree Physiol. 39 (8), 1473–1483. https://doi.org/10.1093/treephys/tpz034.

Collalti, A., Marconi, S., Ibrom, A., Trotta, C., Anav, A., D'andrea, E., Matteucci, G., Montagnani, L., Gielen, B., Mammarella, I., Grünwald, T., Knohl, A., Berninger, F., Zhao, Y., Valentini, R., Santini, M., 2016. Validation of 3D-CMCC Forest Ecosystem Model (v.5.1) against eddy covariance data for 10 European forest sites. Geosci. Model Dev. https://doi.org/10.5194/gmd-9-479-2016.

Collalti, A., Tjoelker, M.G., Hoch, G., Mäkelä, A., Guidolotti, G., Heskel, M., Petit, G., Ryan, M.G., Battipaglia, G., Matteucci, G., Prentice, I.C., 2020. Plant respiration: Controlled by photosynthesis or biomass? Glob. Change Biol. 26 (3), 1739–1753. https://doi.org/10.1111/gcb.14857.

Collalti, A., Dalmonech, D., Vangi, E., Marano, G., Puchi, P.F., Morichetti, M., Saponaro, V., Orrico, M.R., Greco, E., 2024. Monit. Predict. For. Growth Dyn. https://doi.org/10.32018/ForModLab-book-2024.

Collalti, Trotta, C., Keenan, T.F., Ibrom, A., Bond-Lamberty, B., Grote, R., Vicca, S., Reyer, C.P.O., Migliavacca, M., Veroustraete, F., Anav, A., Campioli, M., Scoccimarro, E., Šigut, L., Grieco, E., Cescatti, A., Matteucci, G., 2018. Thinning Can Reduce Losses in Carbon Use Efficiency and Carbon Stocks in Managed Forests Under Warmer Climate. J. Adv. Model. Earth Syst. 10 (10), 2427–2452. https://doi.org/10.1029/2018MS001275.

Conte, A.L., Di Pietro, R., Di Marzio, P., Strumia, S., Cillis, G., Capuano, A., Fortini, P., 2025. Oak decline in southern Italy: environmental and climate parameters for modelling purposes. Veg. Ecol. Divers. 62. https://doi.org/10.3897/ved.160170.

Cornes, R.C., Van Der Schrier, G., Van Den Besselaar, E.J., Jones, P.D., 2018. An ensemble version of the E-OBS temperature and precipitation data sets. J. Geophys. Res. Atmospheres 123 (17), 9391–9409.

Costantini, G., Bellotti, A., Mancino, G., Borghetti, M., 2006. In: Ferrara, A. (Ed.), Carta forestale della Basilicata - Atlante. INEA - Regione, Basilicata, Potenza, p. 99. ISBN 88-8145-062-3.

Costantini, E.A.C., Dazzi, C., 2013. The soils of Italy. Springer, Dordrecht.

Crist, E.P., Cicone, R.C., 1984. Application of the Tasseled Cap concept to simulated thematic mapper data. Photogramm. Eng. Remote Sens. 50 (3), 343–352.

D'Andrea, E., Scartazza, A., Battistelli, A., Collalti, A., Proietti, S., Rezaie, N., Matteucci, G., Moscatello, S., 2021. Unravelling resilience mechanisms in forests: role of non-structural carbohydrates in responding to extreme weather events. Tree Physiol. 41 (10), 1808–1818. https://doi.org/10.1093/treephys/tpab044.

Dalmonech, D., Marano, G., Amthor, J.S., Cescatti, A., Lindner, M., Trotta, C., Collalti, A., 2022. Feasibility of enhancing carbon sequestration and stock capacity in temperate and boreal European forests via changes to management regimes (April). Agric. For. Meteorol. 327, 109203. https://doi.org/10.1016/j.agrformet.2022.109203.

Dalmonech, D., Vangi, E., Chiesi, M., Chirici, G., Fibbi, L., Giannetti, F., Marano, G., Massari, C., Nolè, A., Xiao, J., Collalti, A., 2024. Regional estimates of gross primary production applying the Process-Based Model 3D-CMCC-FEM vs. Remote-Sensing multiple datasets. Eur. J. Remote Sens. 57 (1). https://doi.org/10.1080/22797254.2023.2301657.

De Kroon, H., Van Groenendael, J., Ehrlén, J., 2000. Elasticities: a review of methods and model limitations. Ecology 81 (3), 607–618.

Decarsin, R., Guillemot, J., le Maire, G., Blondeel, H., Meredieu, C., Achard, E., Bonal, D., Cochard, H., Corso, D., Delzon, S., Doucet, Z., Druel, A., Grossiord, C., Torres-Ruiz, J. M., Bauhus, J., Godbold, D.L., Hajek, P., Jactel, H., Jensen, J., Martin-StPaul, N., 2024. Tree drought–mortality risk depends more on intrinsic species resistance than on stand species diversity. Glob. Change Biol. 30 (9). https://doi.org/10.1111/gcb.17503.

van der Maaten, E., Stolz, J., Thurm, E.A., Schröder, J., Henkel, A., Leinemann, L., van der Maaten-Theunissen, M., 2024. Long-term growth decline is not reflected in crown condition of European beech after a recent extreme drought. For. Ecol. Manag. 551, 121516.

DeSoto, L., Cailleret, M., Sterck, F., Jansen, S., Kramer, K., Robert, E.M.R., Aakala, T., Amoroso, M.M., Bigler, C., Camarero, J.J., Čufar, K., Gea-Izquierdo, G., Gillner, S., Haavik, L.J., Hereş, A.-M., Kane, J.M., Kharuk, V.I., Kitzberger, T., Klein, T., Martínez-Vilalta, J., 2020. Low growth resilience to drought is related to future mortality risk in trees. Nat. Commun. 11 (1), 545. https://doi.org/10.1038/s41467-020-14300-5.

Desprez-Loustau, M.-L., Marçais, B., Nageleisen, L.-M., Piou, D., Vannini, A., 2006. Interactive effects of drought and pathogens in forest trees. Ann. For. Sci. 63 (6), 597–612. https://doi.org/10.1051/forest:2006040.

Dorman, M., Perevolotsky, A., Sarris, D., Svoray, T., 2015. The effect of rainfall and competition intensity on forest response to drought: lessons learned from a dry extreme. Oecologia 177 (4), 1025–1038. https://doi.org/10.1007/s00442-015-3229-2.

Duncanson, L., Kellner, J.R., Armston, J., Dubayah, R., Minor, D.M., Hancock, S., Healey, S.P., Patterson, P.L., Saarela, S., Marselis, S., Silva, C.E., Bruening, J., Goetz, S.J., Tang, H., Hofton, M., Blair, B., Luthcke, S., Fatoyinbo, L., Abernethy, K., Zgraggen, C., 2022. Aboveground biomass density models for NASA's Global Ecosystem Dynamics Investigation (GEDI) lidar mission. Remote Sens. Environ. 270, 112845. https://doi.org/10.1016/j.rse.2021.112845.

Fekedulegn, D., Hicks, R.R., Colbert, J.J., 2003. Influence of topographic aspect, precipitation and drought on radial growth of four major tree species in an Appalachian watershed. For. Ecol. Manag. 177 (1–3), 409–425. https://doi.org/10.1016/S0378-1127(02)00446-2.

Forzieri, G., Dakos, V., McDowell, N.G., Ramdane, A., Cescatti, A., 2022. Emerging signals of declining forest resilience under climate change. Nature 608 (7923), 534–539. https://doi.org/10.1038/s41586-022-04959-9.

Friedman, J.H., 2001. Greedy function approximation: a gradient boosting machine. Ann. stat. 1189–1232.

Frieler, K., Volkholz, J., Lange, S., Schewe, J., Mengel, M., del Rocío Rivas López, M., Otto, C., Reyer, C.P.O., Karger, D.N., Malle, J.T., Treu, S., Menz, C., Blanchard, J.L., Harrison, C.S., Petrik, C.M., Eddy, T.D., Ortega-Cisneros, K., Novaglio, C., Rousseau, Y., Bechtold, M., 2024. Scenario setup and forcing data for impact model evaluation and impact attribution within the third round of the Inter-Sectoral Impact Model Intercomparison Project (ISIMIP3a). Geosci. Model Dev. 17 (1), 1–51. https://doi.org/10.5194/gmd-17-1-2024.

Friend, A.D., Eckes-Shephard, A.H., Fonti, P., Rademacher, T.T., Rathgeber, C.B., Richardson, A.D., Turton, R.H., 2019. On the need to consider wood formation processes in global vegetation models and a suggested approach. Ann. For. Sci. 76 (2), 49.

Gazol, A., Camarero, J.J., 2022. Compound climate events increase tree drought mortality across European forests. Sci. Total Environ. 816, 151604. https://doi.org/10.1016/j.scitotenv.2021.151604.

Gazol, A., Ribas, M., Gutiérrez, E., Camarero, J.J., 2017. Aleppo pine forests from across Spain show drought-induced growth decline and partial recovery. Agric. For. Meteorol. 232, 186–194. https://doi.org/10.1016/j.agrformet.2016.08.014.

Gazol, A., Camarero, J.J., Sangüesa-Barreda, G., Serra-Maluquer, X., Sánchez-Salguero, R., Coll, L., Casals, P., 2020. Tree species are differently impacted by cumulative drought stress and present higher growth synchrony in dry places. Front. For. Glob. Change 3, 573346.

Gea-Izquierdo, G., Nicault, A., Battipaglia, G., Dorado-Liñán, I., Gutiérrez, E., Ribas, M., Guiot, J., 2017. Risky future for Mediterranean forests unless they undergo extreme carbon fertilization. Glob. Change Biol. 23 (7), 2915–2927.

Gentilesca, T., Camarero, J.J., Colangelo, M., Nolè, A., Ripullone, F., 2017. Drought-induced oak decline in the western mediterranean region: An overview on current

evidences, mechanisms and management options to improve forest resilience. IForest 10 (5), 796–806. https://doi.org/10.3832/ifor2317-010.
Geri, F., Amici, V., Rocchini, D., 2010. Human activity impact on the heterogeneity of a Mediterranean landscape. Appl. Geogr. 30 (3), 370–379. https://doi.org/10.1016/j.apgeog.2009.10.006.
Gessler, A., Zweifel, R., 2024. Beyond source and sink control – toward an integrated approach to understand the carbon balance in plants. N. Phytol. 242 (3), 858–869. https://doi.org/10.1111/nph.19611.
Gessler, A., Cailleret, M., Joseph, J., Schönbeck, L., Schaub, M., Lehmann, M., Treydte, K., Rigling, A., Timofeeva, G., Saurer, M., 2018. Drought induced tree mortality – a tree-ring isotope based conceptual model to assess mechanisms and predispositions. Source. N. Phytol. 219 (2), 485–490. https://doi.org/10.2307/90022581.
Gonsamo, A., Ciais, P., Miralles, D.G., Sitch, S., Dorigo, W., Lombardozzi, D., Friedlingstein, P., Nabel, J.E.M.S., Goll, D.S., O'Sullivan, M., Arneth, A., Anthoni, P., Jain, A.K., Wiltshire, A., Peylin, P., Cescatti, A., 2021. Greening drylands despite warming consistent with carbon dioxide fertilization effect. Glob. Change Biol. 27 (14), 3336–3349. https://doi.org/10.1111/gcb.15658.
Griffiths, P., van der Linden, S., Kuemmerle, T., Hostert, P., 2013. A pixel-based Landsat compositing algorithm for large area land cover mapping. IEEE J Sel Top Appl Earth Obs Remote Sens 6, 2088–2101. https://doi.org/10.1109/JSTARS.2012.2228167.
Grossiord, C., Bachofen, C., Gisler, J., Mas, E., Vitasse, Y., Didion-Gency, M., 2022. Warming may extend tree growing seasons and compensate for reduced carbon uptake during dry periods. J. Ecol. 110 (7), 1575–1589. https://doi.org/10.1111/1365-2745.13892.
Grünig, M., Rammer, W., Senf, C., Albrich, K., André, F., Augustynczik, A.L., Seidl, R., 2026. Climate change will increase forest disturbances in Europe throughout the 21st century. Science 391 (6789), eadx6329. https://doi.org/10.1126/science.adx6329.
Hammond, W.M., Williams, A.P., Abatzoglou, J.T., Adams, H.D., Klein, T., López, R., Sáenz-Romero, C., Hartmann, H., Breshears, D.D., Allen, C.D., 2022. Global field observations of tree die-off reveal hotter-drought fingerprint for Earth's forests. Nat. Commun. 13 (1). https://doi.org/10.1038/s41467-022-29289-2.
He, W., Liu, H., Qi, Y., Liu, F., Zhu, X., 2020. Patterns in nonstructural carbohydrate contents at the tree organ level in response to drought duration. Glob. Change Biol. 26 (6), 3627–3638. https://doi.org/10.1111/gcb.15078.
Heinrich, S., Yu, X., Limousin, J. -M., Werner, C., Bastos, A., van Dijke, A.H., Walther, S., Kroll, J., Orth, R., 2025. No legacy effects of severe drought on carbon and water fluxes in a Mediterranean oak forest. Plant Biol. https://doi.org/10.1111/plb.70082.
Huang, J., Hammerbacher, A., Gershenzon, J., van Dam, N.M., Sala, A., McDowell, N.G., Chowdhury, S., Gleixner, G., Trumbore, S., Hartmann, H., 2021. Storage of carbon reserves in spruce trees is prioritized over growth in the face of carbon limitation. Proc. Natl. Acad. Sci. 118 (33). https://doi.org/10.1073/pnas.2023297118.
INFC, 2021. Ital. For. Sel. Results Third Natl. For. Inventory. ISBN 978-88-338-5140-2.
IPCC, 2023. Climate Change 2023: Synthesis Report. Contribution of Working Groups I, II and III to the Sixth Assessment Report of the Intergovernmental Panel on Climate Change [Core Writing Team, H. Lee and J. Romero. IPCC, Geneva, Switzerland, pp. 35–115. https://doi.org/10.59327/IPCC/AR6-9789291691647.
Italiano, S.S., Camarero, J.J., Borghetti, M., Colangelo, M., Rita, A., Ripullone, F., 2024. Drought legacies in mixed Mediterranean forests: Analysing the effects of structural overshoot, functional traits and site factors. Sci. Total Environ. 927, 172166.
Jarvis, P., 1976. The interpretation of the variations in leaf water potential and stomatal conductance found in canopies in the field. Philos. Trans. R. Soc. Lond., B Biol. Sci. 273 (927), 593–610.
Jiang, Z., Huete, A., Didan, K., Miura, T., 2008. Development of a two-band enhanced vegetation index without a blue band. Remote Sens. Environ. 112 (10), 3833–3845. https://doi.org/10.1016/j.rse.2008.06.006.
Joffre, R., Rambal, S., Damesin, C., 2007. Functional attributes in Mediterranean-type ecosystems. In: Pugnaire, F., Valladares, F. (Eds.), 'Functional plant ecology', 2nd edn., pp. 285–312.
Kannenberg, S.A., Schwalm, C.R., Anderegg, W.R.L., 2020. Ghosts of the past: how drought legacy effects shape forest functioning and carbon cycling. Ecol. Lett. 23 (5), 891–901. https://doi.org/10.1111/ele.13485.
Klesse, S., DeRose, R.J., Guiterman, C.H., Lynch, A.M., O'Connor, C.D., Shaw, J.D., Evans, M.E., 2018. Sampling bias overestimates climate change impacts on forest growth in the southwestern United States. Nat. commun. 9 (1), 5336.
Knutzen, F., Averbeck, P., Barrasso, C., Bouwer, L.M., Gardiner, B., Grünzweig, J.M., Hänel, S., Haustein, K., Johannessen, M.R., Kollet, S., Müller, M.M., Pietikäinen, J.-P., Pietras-Couffignal, K., Pinto, J.G., Rechid, D., Rousi, E., Russo, A., Suarez-Gutierrez, L., Veit, S., Gliksman, D., 2025. Impacts on and damage to European forests from the 2018–2022 heat and drought events. Nat. Hazards Earth Syst. Sci. 25 (1), 77–117. https://doi.org/10.5194/nhess-25-77-2025.
Koch, J., Demirel, M.C., Stisen, S., 2018. The SPAtial EFficiency metric (SPAEF): Multiple-component evaluation of spatial patterns for optimization of hydrological models. Geosci. Model Dev. 11 (5), 1873–1886.
Lange, S., Menz, C., Gleixner, S., Cucchi, M., Weedon, G.P., Amici, A., Bellouin, N., Müller, Schmied, H., Hersbach, H., Buontempo, C., Cagnazzo, C., 2021. WFDE5 over land merged with ERA5 over the ocean (W5E5 v2.0). ISIMIP Repos. https://doi.org/10.48364/ISIMIP.342217.
Leisenheimer, L., Wellmann, T., Jänicke, C., Haase, D., 2024. Monitoring drought impacts on street trees using remote sensing-Disentangling temporal and species-specific response patterns with Sentinel-2 imagery. Ecol. Inform. 82, 102659.
Lempereur, M., Martin-StPaul, N.K., Damesin, C., Joffre, R., Ourcival, J.M., Rocheteau, A., Rambal, S., 2015. Growth duration is a better predictor of stem increment than carbon supply in a M editerranean oak forest: implications for assessing forest productivity under climate change. N. Phytol. 207 (3), 579–590.
Lhotka, O., Kyselý, J., 2022. The 2021 European Heat Wave in the Context of Past Major Heat Waves. Earth Space Sci. 9 (11). https://doi.org/10.1029/2022EA002567.
Li, X., Xiao, J., 2019b. A global, 0.05-degree product of solar-induced chlorophyll fluorescence derived from OCO-2, MODIS, and reanalysis data. Remote Sens. 11 (5), 517.
Li, X., Xiao, J., 2019. Mapping photosynthesis solely from solar-induced chlorophyll fluorescence: A global, fine-resolution dataset of gross primary production derived from OCO-2. Remote Sens. 11 (21), 2563.
Liaw, A., Wiener, M., 2002. Classification and Regression by randomForest. R. N. 2 (3), 18–22.
Luo, X., Zhao, R., Chu, H., Collalti, A., Fatichi, S., Keenan, T.F., Lu, X., Nguyen, N., Prentice, I.C., Sun, W., Yu, K., Yu, L., 2025. Global variation in vegetation carbon use efficiency inferred from eddy covariance observations. Nat. Ecol. Evol. 9 (8), 1414–1425. https://doi.org/10.1038/s41559-025-02753-0.
Mahnken, M., Cailleret, M., Collalti, A., Trotta, C., Biondo, C., D'Andrea, E., Dalmonech, D., Marano, G., Mäkelä, A., Minunno, F., Peltoniemi, M., Trotsiuk, V., Nadal-Sala, D., Sabaté, S., Vallet, P., Aussenac, R., Cameron, D.R., Bohn, F.J., Grote, R., Reyer, C.P.O., 2022. Accuracy, realism and general applicability of European forest models. Glob. Change Biol. 28 (23), 6921–6943. https://doi.org/10.1111/gcb.16384.
Malle, Johanna T., et al., 2025. "When where High. -Resolut. Clim. data Improv. Impact Model Perform." arXiv Prepr. arXiv 2512, *17739*.
Markuljaková, K., Svitok, M., Mikolás, M., Hofmeister, J., Keeton, W.S., Alhström, A., Ralhan, D., Pavlin, J., Salerno, A.R., Kozák, D., Dúhová, D., Janda, P., Mikac, S., Zlatanov, T., Panayotov, M., Toromani, E., Keren, S., Dikku, A., Roibu, C.-C., Svoboda, M., 2026. Old-growth mixed beech-dominated forests continue accumulating carbon with advancing age. For. Ecosyst. 15, 100411. https://doi.org/10.1016/j.fecs.2025.100411.
Martinez del Castillo, E., Zang, C.S., Buras, A., Hacket-Pain, A., Esper, J., Serrano-Notivoli, R., de Luis, M., 2022. Climate-change-driven growth decline of European beech forests. Commun. Biol. 5 (1), 163.
Martínez-Sancho, E., Treydte, K., Lehmann, M.M., Rigling, A., Fonti, P., 2022. Drought impacts on tree carbon sequestration and water use – evidence from intra-annual tree-ring characteristics. N. Phytol. 236 (1), 58–70. https://doi.org/10.1111/nph.18224.
McDowell, N., Pockman, W.T., Allen, C.D., Breshears, D.D., Cobb, N., Kolb, T., Plaut, J., Sperry, J., West, A., Williams, D.G., Yepez, E.A., 2008. Mechanisms of plant survival and mortality during drought: Why do some plants survive while others succumb to drought? N. Phytol. 178 (4), 719–739. https://doi.org/10.1111/j.1469-8137.2008.02436.x.
Migliavacca, M., Grassi, G., Bastos, A., Ceccherini, G., Ciais, P., Janssens-Maenhout, G., Lugato, E., Mahecha, M.D., Novick, K.A., Peñuelas, J., Pilli, R., Reichstein, M., Avitabile, V., Beck, P.S.A., Barredo, J.I., Forzieri, G., Herold, M., Korosuo, A., Mansuy, N., Cescatti, A., 2025. Securing the forest carbon sink for the European Union's climate ambition. Nature 643 (8074), 1203–1213. https://doi.org/10.1038/s41586-025-08967-3.
Moccia, B., Buonora, L., Bertini, C., Ridolfi, E., Russo, F., Napolitano, F., 2025. What is our pick? Assessment of satellite and reanalysis precipitation datasets over Italy. J. Hydrol. Reg. Stud. 60, 102487.
Molina, M.O., Sánchez, E., Gutiérrez, C., 2020. Future heat waves over the Mediterranean from an Euro-CORDEX regional climate model ensemble. Sci. Rep. 10 (1), 8801. https://doi.org/10.1038/s41598-020-65663-0.
Muñoz-Sabater, J., Dutra, E., Agustí-Panareda, A., Albergel, C., Arduini, G., Balsamo, G., Boussetta, S., Choulga, M., Harrigan, S., Hersbach, H., Martens, B., Miralles, D.G., Piles, M., Rodríguez-Fernández, N.J., Zsoter, E., Buontempo, C., Thépaut, J.N., 2021. ERA5-Land: A state-of-the-art global reanalysis dataset for land applications. Earth Syst. Sci. Data 13 (9), 4349–4383. https://doi.org/10.5194/essd-13-4349-2021.
Neycken, A., Scheggia, M., Bigler, C., Lévesque, M., 2022. Long-term growth decline precedes sudden crown dieback of European beech. Agric. For. Meteorol. 324 (August). https://doi.org/10.1016/j.agrformet.2022.109103.
Neycken, A., Wohlgemuth, T., Frei, E.R., Klesse, S., Baltensweiler, A., Lévesque, M., 2024. Slower growth prior to the 2018 drought and a high growth sensitivity to previous year summer conditions predisposed European beech to crown dieback. Sci. Total Environ. 912, 169068. https://doi.org/10.1016/j.scitotenv.2023.169068.
Nezval, O., Foltýnová, L., Fajstavr, M., Krejza, J., Šigut, L., Světlík, J., Řehořková, Š., Stojanović, M., 2025. Temperature-Driven onset and light quality-linked senescence in *Fagus sylvatica* phenology. Agric. For. Meteorol. 375, 110834. https://doi.org/10.1016/j.agrformet.2025.110834.
Noce, S., Collalti, A., Valentini, R., Santini, M., 2016. Hot spot maps of forest presence in the Mediterranean basin. IForest - Biogeosciences For. 9 (5), 766–774. https://doi.org/10.3832/ifor1802-009.
Noce, S., Collalti, A., Santini, M., 2017. Likelihood of changes in forest species suitability, distribution, and diversity under future climate: The case of Southern Europe. Ecol. Evol. 7 (22), 9358–9375. https://doi.org/10.1002/ece3.3427.
Nolè, A., Collalti, A., Magnani, F., Duce, P., Ferrara, A., Mancino, G., Marras, S., Sirca, C., Spano, D., Borghetti, M., 2013. Assessing temporal variation of primary and ecosystem production in two Mediterranean forests using a modified 3-PG model. Ann. For. Sci. 70 (7), 729–741. https://doi.org/10.1007/s13595-013-0315-7.
Norby, R.J., et al., 2016. Model-data synthesis for the next generation of forest free-air CO2 enrichment (FACE) experiments. N. Phytol. 209, 17–28.
Ossó, A., Allan, R.P., Hawkins, E., Shaffrey, L., Maraun, D., 2022. Emerging new climate extremes over Europe. Clim. Dyn. 58 (1–2), 487–501. https://doi.org/10.1007/s00382-021-05917-3.
Pan, Y., Birdsey, R.A., Phillips, O.L., Houghton, R.A., Fang, J., Kauppi, P.E., Keith, H., Kurz, W.A., Ito, A., Lewis, S.L., Nabuurs, G.J., Shvidenko, A., Hashimoto, S., Lerink, B., Schepaschenko, D., Castanho, A., Murdiyarso, D., 2024. The enduring

world forest carbon sink. Nature 631 (8021), 563–569. https://doi.org/10.1038/s41586-024-07602-x.
Pedersen, B.S., 1998. The role of stress in the mortality of midwestern oaks as indicated by growth prior to death. Ecology 79 (1), 79–93. https://doi.org/10.1890/0012-9658(1998)079[0079:trosit]2.0.co;2.
Peltier, D.M., Ogle, K., 2019. Legacies of more frequent drought in ponderosa pine across the western United States. Glob. Change Biol. 25 (11), 3803–3816.
Peltier, D.M.P., Carbone, M.S., McIntire, C.D., Robertson, N., Thompson, R.A., Malone, S., LeMoine, J., Richardson, A.D., McDowell, N.G., Adams, H.D., Pockman, W.T., Trowbridge, A.M., 2023. Carbon starvation following a decade of experimental drought consumes old reserves in *Pinus edulis*. N. Phytol. 240 (1), 92–104. https://doi.org/10.1111/nph.19119.
Peltier, D.M.P., Nguyen, P., Ebert, C., Koch, G.W., Schuur, E.A.G., Ogle, K., 2024. Moisture stress limits radial mixing of non-structural carbohydrates in sapwood of trembling aspen. Tree Physiol. 44 (13), 204–216. https://doi.org/10.1093/treephys/tpad083.
Petritan, A.M., Petritan, I.C., Hevia, A., Walentowski, H., Bouriaud, O., Sánchez-Salguero, R., 2021. Climate warming predispose sessile oak forests to drought-induced tree mortality regardless of management legacies. For. Ecol. Manag. 491, 119097. https://doi.org/10.1016/j.foreco.2021.119097.
Piovesan, G., Biondi, Filippo, A. di, Alessandrini, S., Maugeri, M., 2008. Drought-driven growth reduction in old beech (*Fagus sylvatica* L.) forests of the central Apennines, Italy. Glob. Change Biol. 14 (6), 1265–1281. https://doi.org/10.1111/j.1365-2486.2008.01570.x.
Piper, F.I., Moreno-Meynard, P., Fajardo, A., 2022. Nonstructural carbohydrates predict survival in saplings of temperate trees under carbon stress. Funct. Ecol. 36 (11), 2806–2818. https://doi.org/10.1111/1365-2435.14158.
Pollastrini, M., Puletti, N., Selvi, F., Iacopetti, G., Bussotti, F., 2019. Widespread crown defoliation after a drought and heat wave in the forests of Tuscany (Central Italy) and their recovery—a case study from summer 2017. Front. For. Glob. Change 2, 74.
Puchi, P.F., Dalmonech, D., Castagneri, D., Genovese, G., Helgason, W., Khomik, M., Brilli, L., Collalti, A., 2026. Decoding carbon allocation in boreal forests: Integrating multi-proxy observations and process-based modelling. Agric. For. Meteorol. 378, 110923. https://doi.org/10.1016/j.agrformet.2025.110923.
Puchi, P.F., Dalmonech, D., Vangi, E., Battipaglia, G., Tognetti, R., Collalti, A., 2024. Contrasting patterns of water use efficiency and annual radial growth among European beech forests along the Italian peninsula. Sci. rep. 14 (1), 6526.
Raffa, M., Reder, A., Adinolfi, M., Mercogliano, P., 2021. A comparison between one-step and two-step nesting strategy in the dynamical downscaling of regional climate model COSMO-CLM at 2.2 km driven by ERA5 reanalysis. Atmosphere 12 (2), 260.
Reyer, 2015. Forest productivity under environmental change—A review of stand-scale modeling studies. Curr. For. Rep. 1 (2), 53–68. https://doi.org/10.1007/s40725-015-0009-5.
Ripullone, F., Camarero, J.J., Colangelo, M., Voltas, J., 2020. Variation in the access to deep soil water pools explains tree-to-tree differences in drought-triggered dieback of mediterranean oaks. Tree Physiol. 40 (5), 591–604. https://doi.org/10.1093/treephys/tpaa026.
Rita, A., Camarero, J.J., Nolè, A., Borghetti, M., Brunetti, M., Pergola, N., Serio, C., Vicente-Serrano, S.M., Tramutoli, V., Ripullone, F., 2020. The impact of drought spells on forests depends on site conditions: The case of 2017 summer heat wave in southern Europe. Glob. Change Biol. 26 (2), 851–863. https://doi.org/10.1111/gcb.14825.
Rosas, T., Galiano, L., Ogaya, R., Peñuelas, J., Martínez-Vilalta, J., 2013. Dynamics of non-structural carbohydrates in three Mediterranean woody species following long-term experimental drought. Front. Plant Sci. 4, 400.
Rubio-Cuadrado, Á., Camarero, J.J., del Río, M., Sánchez-González, M., Ruiz-Peinado, R., Bravo-Oviedo, A., Gil, L., Montes, F., 2018. Drought modifies tree competitiveness in an oak-beech temperate forest. For. Ecol. Manag. 429, 7–17. https://doi.org/10.1016/j.foreco.2018.06.035.
Samaniego, L., Thober, S., Kumar, R., Wanders, N., Rakovec, O., Pan, M., Zink, M., Sheffield, J., Wood, E.F., Marx, A., 2018. Anthropogenic warming exacerbates European soil moisture droughts. Nat. Clim. Change 8 (5), 421–426. https://doi.org/10.1038/s41558-018-0138-5.
Sanginés de Cárcer, P., Vitasse, Y., Peñuelas, J., Jassey, V.E.J., Buttler, A., Signarbieux, C., 2018. Vapor–pressure deficit and extreme climatic variables limit tree growth. Glob. Change Biol. 24 (3), 1108–1122. https://doi.org/10.1111/gcb.13973.
Saponaro, V., Dalmonech, D., Vangi, E., Puchi, P.F., Rezaie, N., D'Andrea, E., Tomelleri, E., Collalti, A., 2025. Climate change, more than management, drives short- and long-term changes in iWUE in a sub-Alpine beech forest. J. For. Res. 37 (1), 16. https://doi.org/10.1007/s11676-025-01942-8.
Schurman, J.S., Babst, F., Björklund, J., Rydval, M., Bače, R., Čada, V., Janda, P., Mikolas, M., Saulnier, M., Trotsiuk, V., Svoboda, M., 2019. The climatic drivers of primary *Picea* forest growth along the Carpathian arc are changing under rising temperatures. Glob. Change Biol. 25 (9), 3136–3150. https://doi.org/10.1111/gcb.14721.
Shestakova, T.A., Gutiérrez, E., Kirdyanov, A.V., Camarero, J.J., Génova, M., Knorre, A. A., Linares, J.C., Resco de Dios, V., Sánchez-Salguero, R., Voltas, J., 2016. Forests synchronize their growth in contrasting Eurasian regions in response to climate warming. Proc. Natl. Acad. Sci. 113 (3), 662–667. https://doi.org/10.1073/pnas.1514717113.
Signarbieux, C., Toledano, E., Sanginés de Carcer, P., Fu, Y.H., Schlaepfer, R., Buttler, A., Vitasse, Y., 2017. Asymmetric effects of cooler and warmer winters on beech phenology last beyond spring. Glob. Change Biol. 23 (11), 4569–4580. https://doi.org/10.1111/gcb.13740.
Sims, D.A., Rahman, A.F., Cordova, V.D., El-Masri, B.Z., Baldocchi, D.D., Flanagan, L.B., … & Xu, L. (2006). On the use of MODIS EVI to assess gross primary productivity of North American ecosystems. *Journal of Geophysical Research: Biogeosciences*, 111 (G4).
Stephenson, N.L., Das, A.J., Condit, R., Russo, S.E., Baker, P.J., Beckman, N.G., Coomes, D.A., Lines, E.R., Morris, W.K., Rüger, N., Álvarez, E., Blundo, C., Bunyavejchewin, S., Chuyong, G., Davies, S.J., Duque, Á., Ewango, C.N., Flores, O., Franklin, J.F., Zavala, M.A., 2014. Rate of tree carbon accumulation increases continuously with tree size. Nature 507 (7490), 90–93. https://doi.org/10.1038/nature12914.
Sterck, F.J., Song, Y., Poorter, L., 2024. Drought- and heat-induced mortality of conifer trees is explained by leaf and growth legacies. Sci. Adv. 10 (15). https://doi.org/10.1126/sciadv.adl4800.
Strobl, C., Boulesteix, A.L., Kneib, T., Augustin, T., Zeileis, A., 2008. Conditional variable importance for random forests. BMC Bioinforma. 9 (1), 307.
Sun, Y., Frankenberg, C., Jung, M., Joiner, J., Guanter, L., Köhler, P., Magney, T., 2018. Overview of Solar-Induced chlorophyll Fluorescence (SIF) from the Orbiting Carbon Observatory-2: Retrieval, cross-mission comparison, and global monitoring for GPP. Remote Sens. Environ. 209, 808–823.
Sun, Z., Wang, X., Zhang, X., Tani, H., Guo, E., Yin, S., Zhang, T., 2019. Evaluating and comparing remote sensing terrestrial GPP models for their response to climate variability and CO2 trends. Sci. Total Environ. 668, 696–713.
Svensson, J., Jonsson, B.G., Ebenhard, T., 2025. The EU Nature Restoration Regulation offers new opportunities for resilient forests and sustainable forestry. Ambio. https://doi.org/10.1007/s13280-025-02309-3.
Testolin, R., Dalmonech, D., Marano, G., D'Andrea, E., Matteucci, G., Noce, S., Collalti, A., 2023. Simulating diverse forest management in a changing climate on a Pinus nigra subsp. Laricio plantation in Southern Italy. Sci. Total Environ. 857, 159361. https://doi.org/10.1016/j.scitotenv.2022.159361.
Tramblay, Y., Koutroulis, A., Samaniego, L., Vicente-Serrano, S.M., Volaire, F., Boone, A., Le Page, M., Llasat, M.C., Albergel, C., Burak, S., Cailleret, M., Kalin, K.C., Davi, H., Dupuy, J.-L., Greve, P., Grillakis, M., Hanich, L., Jarlan, L., Martin-StPaul, N., Polcher, J., 2020. Challenges for drought assessment in the Mediterranean region under future climate scenarios. Earth-Sci. Rev. 210, 103348. https://doi.org/10.1016/j.earscirev.2020.103348.
Vanella, D., Longo-Minnolo, G., Belfiore, O.R., Ramírez-Cuesta, J.M., Pappalardo, S., Consoli, S., Gandolfi, C., 2022. Comparing the use of ERA5 reanalysis dataset and ground-based agrometeorological data under different climates and topography in Italy. J. Hydrol. Reg. Stud. 42, 101182.
Vangi, E., Dalmonech, D., Cioccolo, E., Marano, G., Bianchini, L., Puchi, P.F., Grieco, E., Cescatti, A., Colantoni, A., Chirici, G., Collalti, A., 2024. Stand age diversity (and more than climate change) affects forests' resilience and stability, although unevenly. J. Environ. Manag. 366, 121822. https://doi.org/10.1016/J.JENVMAN.2024.121822.
Vangi, E., Dalmonech, D., d'Amico, G., Grieco, E., Morichetti, M., Puchi, P.F., Francini, S., Fares, S., Giannetti, F., Corona, P., Barbetti, R., Chirici, G., Collalti, A., 2025. Monitoring forest attributes, C-fluxes, and C-stocks using the process-based model 3D-CMCC-FEM at the National level. Ecol. Inform. 92, 103489. https://doi.org/10.1016/j.ecoinf.2025.103489.
Vayreda, J., Martinez-Vilalta, J., Gracia, M., Retana, J., 2012. Recent climate changes interact with stand structure and management to determine changes in tree carbon stocks in <scp>S</scp> panish forests. Glob. Change Biol. 18 (3), 1028–1041. https://doi.org/10.1111/j.1365-2486.2011.02606.x.
Vicente-Serrano, S.M., Beguería, S., López-Moreno, J.I., 2010. A Multiscalar Drought Index Sensitive to Global Warming: The Standardized Precipitation Evapotranspiration Index. J. Clim. 23 (7), 1696–1718. https://doi.org/10.1175/2009JCLI2909.1.
Vicente-Serrano, S.M., Martín-Hernández, N., Camarero, J.J., Gazol, A., Sánchez-Salguero, R., Peña-Gallardo, M., El Kenawy, A., Domínguez-Castro, F., Tomas-Burguera, M., Gutiérrez, E., de Luis, M., Sangüesa-Barreda, G., Novak, K., Rozas, V., Tíscar, P.A., Linares, J.C., del Castillo, E.M., Ribas, M., García-González, I., Diego Galván, J., 2020. Linking tree-ring growth and satellite-derived gross primary growth in multiple forest biomes. Temporal-scale matters. Ecol. Indic. 108, 105753. https://doi.org/10.1016/j.ecolind.2019.105753.
Wang, X., Xu, T., Xu, C., Liu, H., Chen, Z., Li, Z., Li, X., Wu, X., 2024. Enhanced growth resistance but no decline in growth resilience under long-term extreme droughts. Glob. Change Biol. 30 (1). https://doi.org/10.1111/gcb.17038.
White, J.C., Wulder, M.A., Hobart, G.W., Luther, J.E., Hermosilla, T., Griffiths, P., Guindon, L., 2014. Pixel-based image compositing for large-area dense time series applications and science. Can. J. Remote Sens. 40 (3), 192–212.
Xu, P., Wang, L., Liu, Y., Chen, W., Huang, P., 2020. The record-breaking heat wave of June 2019 in Central Europe. Atmos. Sci. Lett. 21 (4). https://doi.org/10.1002/asl.964.
Xue, J., Su, B., 2017. Significant Remote Sensing Vegetation Indices: A Review of Developments and Applications. J. Sens. 2017, 1–17. https://doi.org/10.1155/2017/1353691.
Yan, Y., Piao, S., Hammond, W.M., Chen, A., Hong, S., Xu, H., Allen, C.D., 2024. Climate-induced tree-mortality pulses are obscured by broad-scale and long-term greening. Nat. Ecol. Evol. 8 (5), 912–923.
Yuan, W., Zheng, Y., Piao, S., Ciais, P., Lombardozzi, D., Wang, Y., Ryu, Y., Chen, G., Dong, W., Hu, Z., Jain, A.K., Jiang, C., Kato, E., Li, S., Lienert, S., Liu, S., Nabel, J.E. M.S., Qin, Z., Quine, T., Yang, S., 2019. Increased atmospheric vapor pressure deficit reduces global vegetation growth. Sci. Adv. 5 (8). https://doi.org/10.1126/sciadv.aax1396.

Yue, S., Pilon, P., Phinney, B., Cavadias, G., 2002. The influence of autocorrelation on the ability to detect trend in hydrological series. Hydrol. Process. 16 (9), 1807–1829.
Zhu, Z., Piao, S., Myneni, R.B., Huang, M., Zeng, Z., Canadell, J.G., Ciais, P., Sitch, S., Friedlingstein, P., Arneth, A., Cao, C., Cheng, L., Kato, E., Koven, C., Li, Y., Lian, X., Liu, Y., Liu, R., Mao, J., Zeng, N., 2016. Greening of the Earth and its drivers. Nat. Clim. Change 6 (8), 791–795. https://doi.org/10.1038/nclimate3004.
Zweifel, R., Sterck, F., 2018. A conceptual tree model explaining legacy effects on stem growth. Front. For. Glob. Change 1. https://doi.org/10.3389/ffgc.2018.00009.